



An antiproliferative BMP-2/PPAR γ /apoE axis in human and murine SMCs and its role in pulmonary hypertension

Georg Hansmann,^{1,2} Vinicio A. de Jesus Perez,¹ Tero-Pekka Alastalo,¹ Cristina M. Alvira,¹ Christophe Guignabert,¹ Janine M. Bekker,¹ Stefan Schellong,¹ Takashi Urashima,¹ Lingli Wang,¹ Nicholas W. Morrell,³ and Marlene Rabinovitch¹

¹Department of Pediatrics, Stanford University School of Medicine, Stanford, California, USA. ²Department of Pediatrics, UCSF, San Francisco, California, USA. ³Department of Medicine, University of Cambridge, Cambridge, United Kingdom.

Loss-of-function mutations in bone morphogenetic protein receptor II (BMP-RII) are linked to pulmonary arterial hypertension (PAH); the ligand for BMP-RII, BMP-2, is a negative regulator of SMC growth. Here, we report an interplay between PPAR γ and its transcriptional target apoE downstream of BMP-2 signaling. BMP-2/BMP-RII signaling prevented PDGF-BB-induced proliferation of human and murine pulmonary artery SMCs (PASMCs) by decreasing nuclear phospho-ERK and inducing DNA binding of PPAR γ that is independent of Smad1/5/8 phosphorylation. Both BMP-2 and a PPAR γ agonist stimulated production and secretion of apoE by SMCs. Using a variety of methods, including short hairpin RNAi in human PASMCs, PAH patient-derived BMP-RII mutant PASMCs, a PPAR γ antagonist, and PASMCs isolated from PPAR γ - and apoE-deficient mice, we demonstrated that the antiproliferative effect of BMP-2 was BMP-RII, PPAR γ , and apoE dependent. Furthermore, we created mice with targeted deletion of PPAR γ in SMCs and showed that they spontaneously developed PAH, as indicated by elevated RV systolic pressure, RV hypertrophy, and increased muscularization of the distal pulmonary arteries. Thus, PPAR γ -mediated events could protect against PAH, and PPAR γ agonists may reverse PAH in patients with or without BMP-RII dysfunction.

Introduction

Bone morphogenetic protein 2 (BMP-2) is a negative regulator of SMC growth, but the mechanism by which it counteracts proliferation induced by growth factors (i.e., PDGF-BB, EGF) associated with pulmonary arterial hypertension (PAH) (1, 2) remains to be characterized. Loss-of-function-mutations in the BMP receptor II (BMP-RII) gene occur in 50%–60% of patients with familial PAH (FPAH) (3–5), 10%–20% of patients with idiopathic PAH (IPAH), and 6%–9% of patients with secondary forms of PAH associated with anorexic drug use (fenfluramine derivatives) or congenital heart defects (APAH) (6, 7). However, independent of a mutation, patients with IPAH/FPAH (formerly called “primary PH”), and even those with APAH (formerly called “secondary” PAH), albeit to a lesser extent, have reduced pulmonary expression of BMP-RII (8). Thus, there are likely environmental modifiers and additional genetic factors that contribute to the decreased expression and function of BMP-RII in association with the development of PAH. This would suggest that it might be possible to rescue the adverse sequelae of reduced expression and antimitogenic signaling of BMP-RII by manipulating its downstream effectors to advantage.

Two potential downstream effectors of BMP-RII signaling are the transcription factor PPAR γ and its putative target apoE (9). Interestingly, mRNA expression of both factors, in addition to BMP-2, is decreased in lung tissues from PAH patients (8, 10, 11). PPARs are ligand-activated transcription factors belonging to the nuclear

receptor superfamily. Upon ligand activation, PPARs heterodimerize with the retinoid X receptor (RXR) and bind to PPAR response elements (PPREs) in regulatory promoter regions of their target genes (12, 13). PPARs can also interact with signaling molecules to regulate gene expression independent of DNA binding (13). For example, PPAR γ impairs phosphorylation (i.e., activation) of ERK (14, 15), a MAPK downstream of PDGF-BB/PDGFR- β signaling implicated in SMC proliferation and migration (12).

There is supporting evidence that links PPAR γ with transcription of apoE. A functional PPAR γ response element is present in the apoE promoter (9), conditional disruption of the PPAR γ gene (*Pparg*) in mice results in decreased apoE expression in macrophages (16), and PPAR γ activation leads to apoE mRNA expression and protein secretion in an adipocyte cell line (17). apoE inhibits PDGF-BB-mediated SMC proliferation and migration (18, 19) by binding to LDL receptor-related protein (LRP) and internalizing the PDGFR- β (20, 21). Heightened arterial PDGF-BB/MAPK signaling is not only evident in apoE^{-/-} mice (22), but is also a key clinical feature of pulmonary vascular disease underlying PAH (2, 23, 24).

We have recently shown that insulin-resistant apoE-deficient (apoE^{-/-}) mice on a high-fat diet develop PAH. However, the fact that a PPAR γ agonist reversed PAH in this model (25) suggests that PPAR γ targets independent of apoE are also important in suppressing pulmonary vascular remodeling. The antidiabetic drugs rosiglitazone and pioglitazone, both PPAR γ ligands of the thiazolidinedione (TZD) class, inhibit PDGF-BB-induced SMC proliferation and migration in culture and in animal models of systemic cardiovascular disease (reviewed in ref. 12). Because of these and additional antiinflammatory and proapoptotic effects of PPAR γ activation (reviewed in ref. 12), PPAR γ agonists may be useful in the future treatment of PAH.

Nonstandard abbreviations used: BMP-2, bone morphogenetic protein 2; BMP-RII, BMP receptor II; FPAH, familial PAH; HPASMC, human PASMC; PAH, pulmonary arterial hypertension; PASMC, pulmonary artery SMC; RVSP, RV systolic pressure.

Conflict of interest: The authors have declared that no conflict of interest exists.

Citation for this article: *J. Clin. Invest.* 118:1846–1857 (2008). doi:10.1172/JCI32503.



Here, we report for the first time to our knowledge that both PPAR γ and apoE act downstream of BMP-2/BMP-RII in primary cells (human and murine pulmonary artery SMCs [PASCs]) and prevent SMC proliferation in response to PDGF-BB. BMP-2-mediated PPAR γ activation occurs earlier than Smad1/5/8 phosphorylation and therefore appears to be independent of this established signaling axis downstream of BMP-RII. BMP-2 induces a decrease in nuclear phospho-ERK, and rapid nuclear shuttling and DNA binding of PPAR γ , whereas PDGF-BB has the opposite effects. Both BMP-2 and the PPAR γ agonist rosiglitazone stimulate production and secretion of apoE in PASCs. Using short hairpin RNAi in human PASCs (HPASCs), PASCs from a patient with FPAH and a mutation in BMP-RII (W9X), a PPAR γ antagonist, and PASCs lacking PPAR γ or apoE, we demonstrate that the antiproliferative effect of BMP-2 is BMP-RII, PPAR γ , and apoE dependent. Consistent with these data, we show that mice with deletion of PPAR γ in SMCs (*SM22 α Cre PPAR $\gamma^{flox/flox}$* mice) spontaneously develop PAH. Taken together, our results reveal a novel PPAR γ /apoE axis downstream of BMP-2 signaling that could explain the antiproliferative effect of BMP-RII activation in HPASCs. Our data also suggest that PPAR γ agonists might reverse SMC proliferation and vascular remodeling in PAH patients with or without BMP-RII dysfunction.

Results

Additional results are provided in the supplemental material (available online with this article; doi:10.1172/JCI32503DS1).

BMP-2-mediated inhibition of HPASC proliferation requires BMP-RII, PPAR γ , and apoE. For long-term gene silencing of human BMP-RII, we constructed a pLentivirus 6 with an integrated short hairpin oligonucleotide directed against the mRNA of human BMP-RII (shRNAi). We confirmed, by quantitative RT-PCR, an 85% stable knockdown of BMP-RII mRNA in shBMP-RII versus shLacZi (control) transfected HPASCs (Supplemental Figure 1). Recombinant BMP-2 (10 ng/ml) inhibited PDGF-BB-induced proliferation in LacZi control but not in shBMP-RII HPASCs as judged by cell counts (Figure 1). Results of MTT proliferation assays shown in Supplemental Figure 2 are consistent with cell counts. We reproduced the growth-inhibitory effect of BMP-2, with the same low concentration (10 ng/ml) of BMP-4 and -7, although BMP-7 appeared to have a weaker effect than BMP-2 and -4. Furthermore, with siBMP-RII (knockdown), there was less growth inhibition in response to BMP-2, -4, and -7 (Supplemental Figure 3). We also confirmed that siBMP-RII abolished BMP-2-induced phosphorylation of Smad1/5/8 (Supplemental Figure 4).

We then showed that the BMP-2-mediated inhibition of PDGF-BB-induced HPASC proliferation requires not only BMP-RII, but also PPAR γ . First, the antimitogenic effect of BMP-2 could be reproduced by the PPAR γ agonist rosiglitazone (1 μ M) (Figure 1B). Second, the antiproliferative effect of BMP-2 was lost in the presence of the irreversible PPAR γ antagonist GW9662 (Figure 1C). Finally, BMP-2-mediated inhibition of PDGF-BB-induced cell proliferation was not observed in murine PASCs with deletion of PPAR γ but was found in PASCs from littermate controls (Figure 1D). To address whether the effect of PPAR γ could be mediated by induction of apoE, we first established that a physiological dose of recombinant apoE (10 μ M) completely blocked PDGF-BB-induced proliferation of HPASCs (Figure 1E). Moreover, the growth-inhibitory effect of BMP-2 on PDGF-BB-induced cell proliferation was lost in PASCs from apoE $^{-/-}$ mice (Figure 1F). Taken together, these data support the presence of a novel

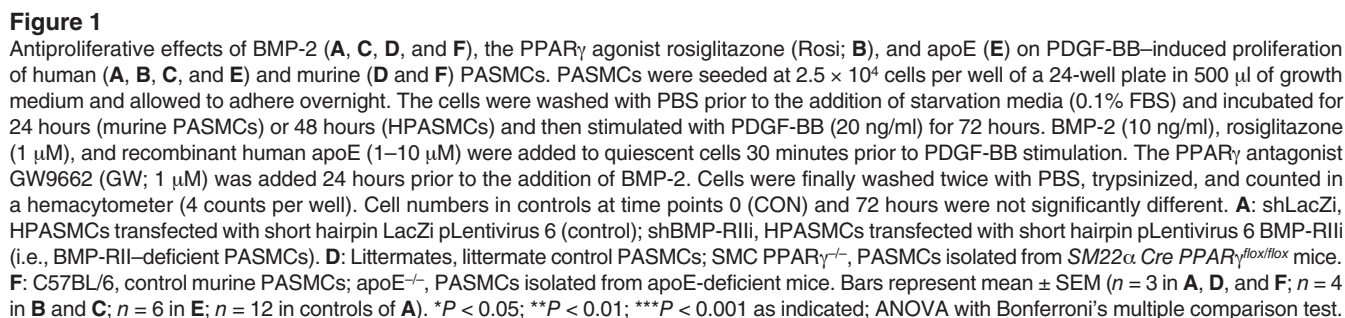
antiproliferative axis downstream of BMP-2 that requires BMP-RII signaling, PPAR γ activation, and production of apoE, a lipoprotein not previously known to be synthesized by SMC. Documentation of apoE production and secretion in HPASCs in response to BMP-2 and rosiglitazone is described below.

Opposing effects of PDGF-BB and BMP-2 on phospho-ERK and PPAR γ activation in HPASCs. We next determined whether BMP-2 and PDGF-BB might have opposing effects on the subcellular localization of phospho-ERK and PPAR γ that would explain their functional antagonism in PASCs. PPAR γ has been shown to activate phosphatases and prevent ERK phosphorylation in vascular SMCs (14, 15). In addition, PPAR γ activation can directly inhibit PDGF-BB-mediated phospho-ERK activity (26) by blocking its nuclear translocation (27). Conversely, PDGF-BB/PDGFR- β -mediated phosphorylation of ERK leads to phosphorylation and thereby inactivation of PPAR γ at its N terminus (28).

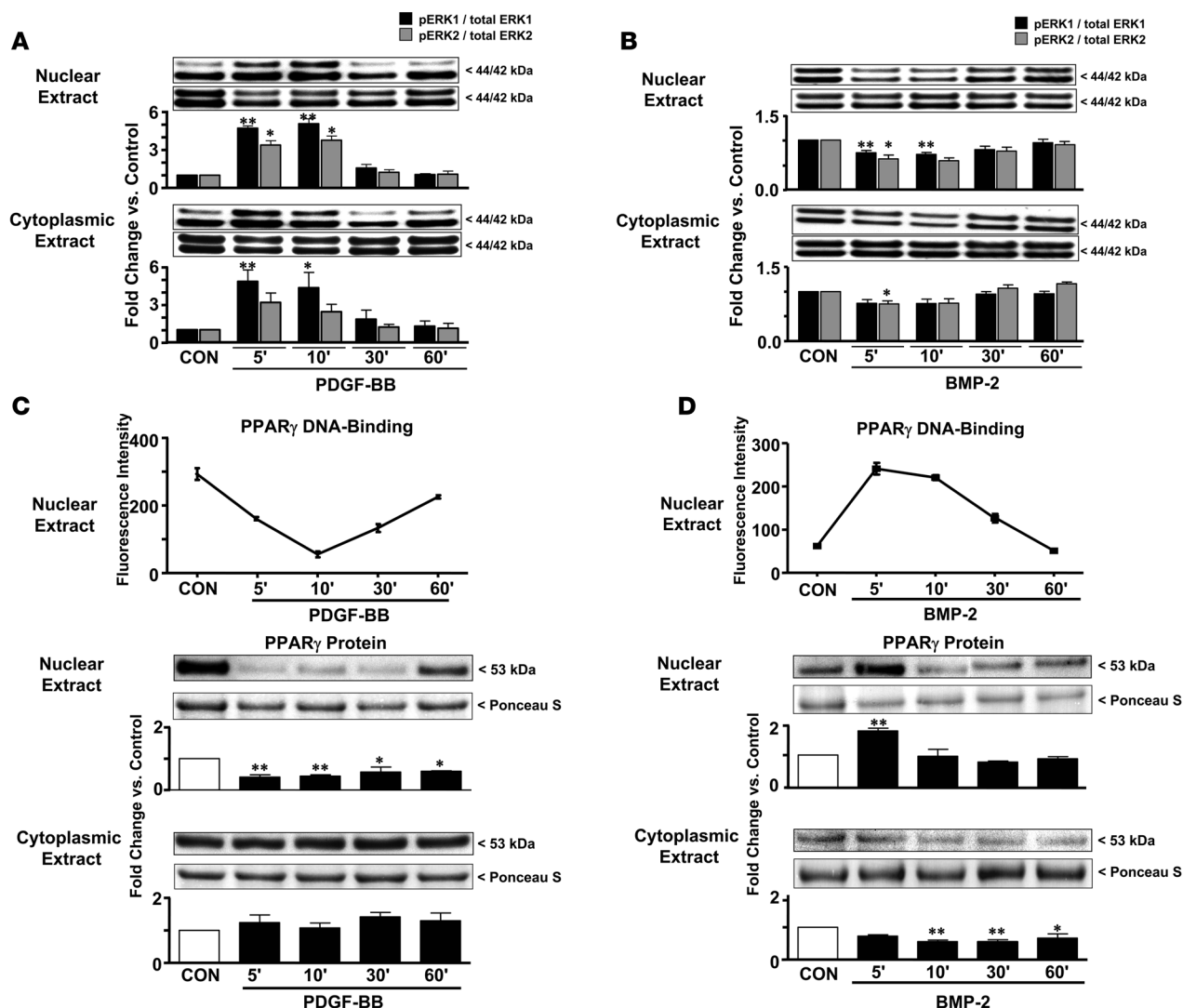
PDGF-BB stimulated a 3- to 5-fold increase in phospho-ERK1/2 in nuclear extracts and a 4-fold rise in phospho-ERK1 in cytoplasmic extracts (Figure 2A). BMP-2, however, led to a rapid decrease in phospho-ERK1/2 in nuclear extracts (Figure 2B) and significantly reduced phospho-ERK2 in cytoplasmic extracts (Figure 2B). PDGF-BB rapidly and transiently decreased nuclear protein levels and DNA binding of PPAR γ . This decrease in PPAR γ DNA binding (Figure 2C, upper panel) temporally coincided with the rapid appearance of phospho-ERK1/2 in the nucleus upon PDGF-BB stimulation (maximum at 5–10 min; Figure 2A). There was no significant change in PPAR γ levels in cytoplasmic extracts (Figure 2C). In contrast to PDGF-BB, BMP-2 induced a rapid and marked increase in PPAR γ DNA binding (Figure 2D) associated with elevated levels of PPAR γ protein in nuclear extracts. This could represent stabilization of PPAR γ , but since PPAR γ tended to be concomitantly lower in cytoplasmic extracts, transient nuclear shuttling of PPAR γ is also likely (Figure 2D). Of note, BMP-2-mediated PPAR γ activation in HPASCs (Figure 2, B and D) occurred earlier than phosphorylation of Smad1/5/8 (Supplemental Figure 4). Therefore, phospho-Smad1/5/8 does not appear to mediate DNA binding of PPAR γ .

Interestingly, when we prepared total cell lysates containing the cytoplasmic membrane fraction, we found that BMP-2 induces rapid ERK1/2 phosphorylation (Supplemental Figure 5A). This fraction is absent in nuclear and cytoplasmic extract preparations due to high spin steps. We showed by immunohistochemistry that concomitant with the rapid decrease in phospho-ERK1/2 in the nucleus (shown by Western immunoblot in Figure 2B), BMP-2 led to strong phospho-ERK1/2 staining at the cytoplasmic membrane (Supplemental Figure 5B). It has been previously demonstrated in other cell types that phospho-ERK binds to cytoplasmic membrane proteins such as the receptor for advanced glycation end products (29).

BMP-2 and a PPAR γ agonist inhibit PDGF-BB signaling in HPASCs. We next determined whether BMP-2 and PPAR γ activation inhibit PDGF-BB-induced MAPK pathways (i.e., phospho-ERK1/2). BMP-2 inhibited PDGF-BB-induced nuclear and cytoplasmic ERK phosphorylation (Figure 3A). BMP-2 also prevented PDGF-BB-mediated inhibition of PPAR γ DNA binding. In fact an increase in PPAR γ DNA binding was observed with BMP-2 despite concomitant PDGF-BB stimulation (Figure 3B). Moreover, 24-hour preincubation with the PPAR γ agonist rosiglitazone significantly reduced and delayed PDGF-BB-induced ERK phosphorylation in total cell lysates (Figure 3C). Hence, BMP-2 and the PPAR γ agonist rosiglitazone act as functional antagonists of PDGF-BB signaling by inhibiting ERK1/2 phosphorylation.



to harbor a frameshift mutation in BMP-RII. BMP-2 inhibited PDGF-BB-induced proliferation in WT but not BMP-RII mutant HPASMCs (Figure 4). In contrast, the PPAR γ agonist rosiglitazone blocked PDGF-BB-induced proliferation in both WT and BMP-RII mutant cells so that cell numbers were similar to those in unstim-

**Figure 2**

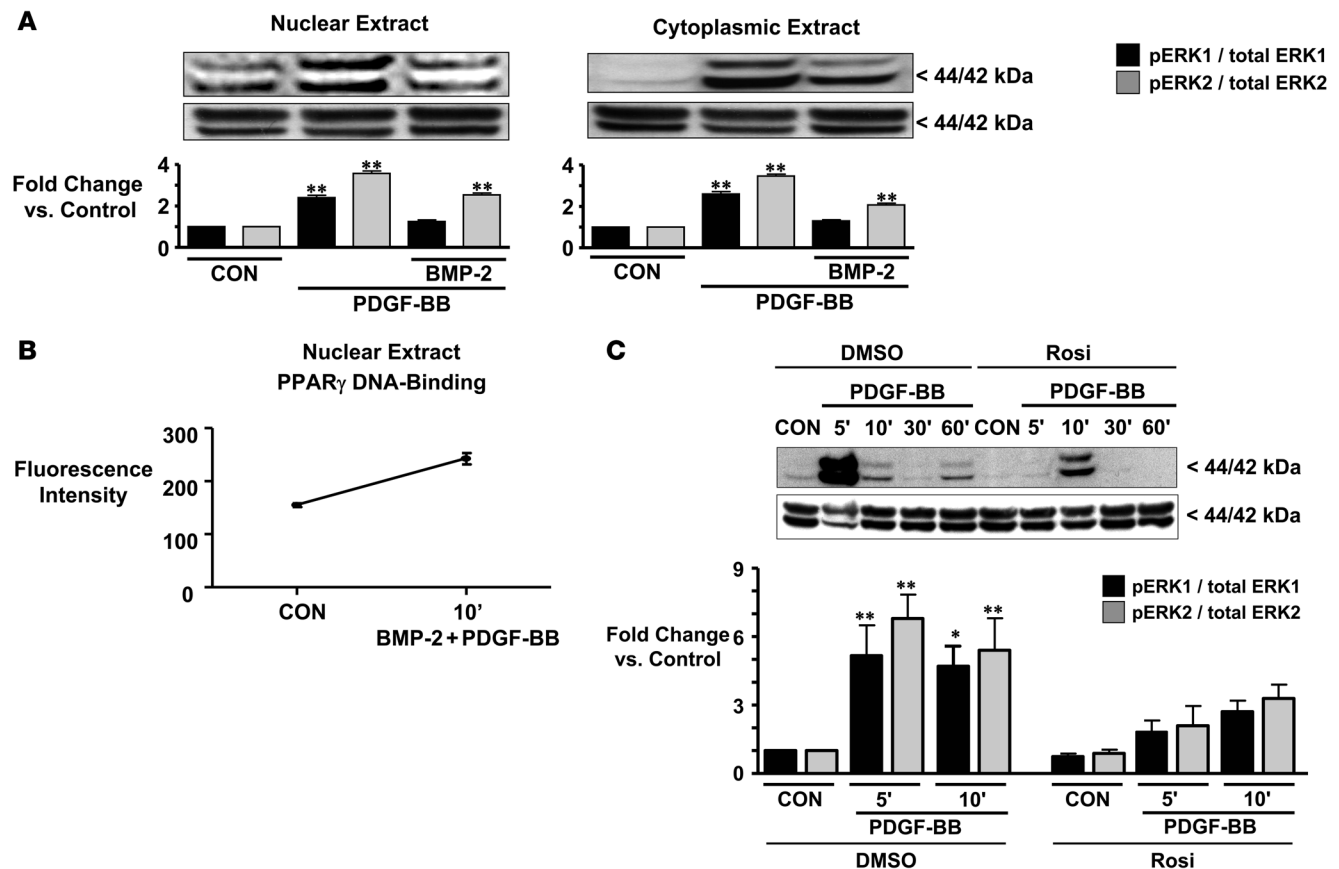
PDGF-BB (A and C) and BMP-2 (B and D) have opposing effects in HPASMCs on protein levels of phospho-ERK/total ERK (A and B), PPAR γ DNA binding in nuclear extracts (upper panels in C and D), and PPAR γ protein in nuclear and cytoplasmic extracts (lower panels in C and D). Cells were stimulated with PDGF-BB (20 ng/ml) or BMP-2 (10 ng/ml) as described in the legend for Figure 1. In separate experiments, we determined that neither of the solvents (DMSO, sterile water; both 1:10,000) influenced the results. Western immunoblotting and PPAR γ DNA binding assays are described in Methods. For the PPAR γ DNA binding assay, bars represent median \pm SEM of triplicate measurements of 1 representative experiment of 2 (C) and 3 (D) independent experiments with similar results. For protein levels in cell fractions, bars represent mean \pm SEM ($n = 3-4$). * $P < 0.05$; ** $P < 0.01$ versus control; ANOVA with Dunnett's post-hoc test.

ulated controls (Figure 4). BMP-2 and rosiglitazone, in the (low) concentrations used, had no significant effect on the basal cell proliferation rate (Figure 4). Thus, PPAR γ agonists have the potential to rescue the growth-inhibitory effect of BMP-2 in PSMCs with BMP-RII dysfunction.

BMP-2 and rosiglitazone induce apoE expression and secretion in HPASMCs. Since the growth-inhibitory effect of BMP-2 is absent in apoE-deficient PSMCs (Figure 1F), we hypothesized that apoE might be a transcriptional target of BMP-2-activated PPAR γ in SMCs. Indeed, both BMP-2 and rosiglitazone induced apoE protein expression (cell lysates) and secretion (supernatant) in HPASMCs (Figure 5A). Moreover, the BMP-2-mediated upregulation of apoE protein was reduced by half in PSMCs harvested from *SM22 α Cre*

PPAR γ ^{flox/flox} mice (Figure 5B). This suggests that the induction of apoE expression by BMP-2 is to a great extent PPAR γ dependent.

Creation of mice with targeted deletion of PPAR γ in arterial SMCs (*SM22 α Cre PPAR γ ^{flox/flox}*). To explore the vasoprotective role of PPAR γ in preventing the development of PAH in an intact animal, we investigated a transgenic mouse with targeted deletion of PPAR γ in arterial SMCs (*SM22 α Cre PPAR γ ^{flox/flox}*). We documented, by PCR, gain of a new knockout transcript (300 bp) and almost complete loss of the 700-bp wild-type transcript in PSMCs and aorta isolated from *SM22 α Cre PPAR γ ^{flox/flox}* mice (Figure 6A). Both the wild-type and the knockout transcript were found in lungs from *SM22 α Cre PPAR γ ^{flox/flox}* mice, since the tissue contains several cell types besides SMCs. In contrast, only the wild-type transcript was detected in lung

**Figure 3**

BMP-2 and rosiglitazone inhibit PDGF-BB-mediated ERK phosphorylation (A and C), and concomitant BMP-2 and PDGF-BB stimulation increases PPAR γ DNA binding (B), in HPASMCs. Cells were preincubated with BMP-2 (10 ng/ml) for 30 minutes (A and B) or rosiglitazone (1 μ M) for 24 hours (C), followed by PDGF-BB (20 ng/ml) stimulation for 10 minutes (A and B) or 5–60 minutes (C). Western immunoblotting and PPAR γ DNA binding assays are described in Methods and Figure 2. For protein levels in cell fractions (A) or cell lysates (C), bars represent mean \pm SEM ($n = 3$ each). In C, all samples are compared with the DMSO control. For the PPAR γ DNA binding assay (B), bars represent median \pm SEM of triplicate measurements of 1 representative experiment of 3 independent experiments with similar results. * $P < 0.05$; ** $P < 0.01$ versus control; ANOVA with Dunnett's post-hoc test.

tissue from littermate control mice (Figure 6A). We also confirmed knockout of PPAR γ protein in PSMCs from *SM22 α Cre PPAR $\gamma^{flox/flox}$* mice (Figure 6B). BMP-2 stimulation of these murine PPAR γ -deficient PSMCs revealed intact phospho-Smad1/5/8 signaling that occurred earlier (5–10 minutes; Figure 6C) than in human control PSMCs, where it was observed at 30 minutes (Supplemental Figure 4). Hence, the established BMP-2/phospho-Smad1/5/8 signaling pathway appears to be independent of PPAR γ , since it occurs in PSMCs with deletion of PPAR γ (Figure 6C).

Mice with targeted deletion of PPAR γ in arterial SMCs (*SM22 α Cre PPAR $\gamma^{flox/flox}$*) have PAH. *SM22 α Cre PPAR $\gamma^{flox/flox}$* mice had elevated RV systolic pressure (RVSP) in room air when compared with controls (29.0 versus 21.5 mmHg; $P < 0.001$; Figure 7A). Systemic blood pressure, RV function (RV dP/dt maximum and minimum) and LV function (fractional shortening, ejection fraction), and cardiac output were not significantly different when comparing the 2 groups (Table 1). In association with elevated RVSP as a measure of PAH, *SM22 α Cre PPAR $\gamma^{flox/flox}$* mice also developed RV hypertrophy (RVH), as judged by the ratio of RV weight to that of the LV and septum (0.46 versus 0.26; $P < 0.0001$; Figure 7B) and the ratio of RV to body weight ($P < 0.001$; Table 1). *SM22 α Cre PPAR $\gamma^{flox/flox}$* mice had a similar number of pul-

monary arteries per 100 alveoli (Table 1) and per surface area (data not shown) but showed more muscularized pulmonary arteries at the alveolar wall level, when compared with littermate controls (Figure 7, C–E). The muscular thickening in small pulmonary arteries seen in lung sections from SMC PPAR γ -deficient mice (Movat staining; Figure 7, D and E) was confirmed by immunohistochemistry with specific antibodies for α -SMA (Figure 7, F and G) and associated with an enhanced signal for proliferating cell nuclear antigen (PCNA; Figure 7, H and I) in PSMCs. LV end-diastolic inner diameter (LVIDD), LV end-diastolic posterior wall thickness (LVPWd), and end-diastolic interventricular septum thickness (IVSd) as measures of LV dilatation and LV hypertrophy (LVH) were not different between the 2 genotypes (Table 1). Thus, LV dysfunction does not account for the PAH in *SM22 α Cre PPAR $\gamma^{flox/flox}$* mice. *SM22 α Cre PPAR $\gamma^{flox/flox}$* mice had similar hematocrit and glucose values but slightly higher wbc counts than controls (Table 1).

Discussion

This report is the first indication to our knowledge that the anti-proliferative effects of BMP-2/BMP-RII signaling in primary cells (i.e., PSMCs) can be attributed to activation of PPAR γ and its

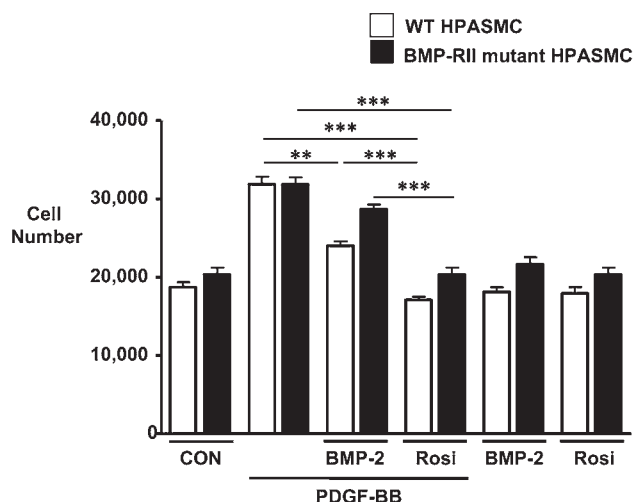


Figure 4

Antiproliferative effects of BMP-2 and the PPAR γ agonist rosiglitazone on PDGF-BB-induced proliferation of human wild-type and BMP-II mutant PSMCs. Control PSMCs were isolated from surgical resection specimens derived from patients undergoing lobectomy or pneumonectomy for suspected lung tumor. Additional peripheral pulmonary arteries (<1–2 mm external diameter) were obtained from a patient undergoing heart-lung transplantation for FPAH and known to harbor a mutation (W9X) in BMP-II. The nature of the BMP-II mutation, cell isolation, culture techniques, and cell counts are described in Methods and in Figure 1. HPASMCs were incubated for 48 hours in starvation media (0.1% FBS) and then stimulated with PDGF-BB (20 ng/ml) for 72 hours. BMP-2 (10 ng/ml) or rosiglitazone (1 μ M) were added to quiescent cells 30 minutes prior to PDGF-BB stimulation. Bars represent mean \pm SEM ($n = 3$). ** $P < 0.01$; *** $P < 0.001$ as indicated; ANOVA with Bonferroni's multiple comparison test. The number of PDGF-BB-stimulated cells was significantly higher than that of untreated control cells ($P < 0.001$).

putative transcription target apoE, a protein not previously known to be synthesized and secreted by SMCs (Figure 8A). Furthermore, we establish that endogenous expression of PPAR γ in SMCs can protect against the spontaneous development of PAH. Our experiments using a PPAR γ antagonist and PPAR γ -deficient PSMCs further demonstrate that PPAR γ is required for BMP-2-mediated inhibition of PSMC proliferation induced by PDGF-BB. By using RNAi and PSMCs with a known loss-of-function mutation of BMP-II, we show that BMP-2 requires BMP-II to block SMC

proliferation and provide evidence that BMP-II dysfunction that occurs with or without BMP-II mutations (3, 4) could lead to unopposed mitogenic SMC stimulation by PDGF-BB and other growth factors (Figure 8B). BMP-II dysfunction may, however, be rescued by PPAR γ agonists such as pioglitazone or rosiglitazone (Figure 8C), as we have demonstrated in PDGF-BB-stimulated BMP-II mutant HPASMCs.

In this study, we investigated whether BMP-2 and PDGF-BB might have opposing effects on the growth-inhibitory transcrip-

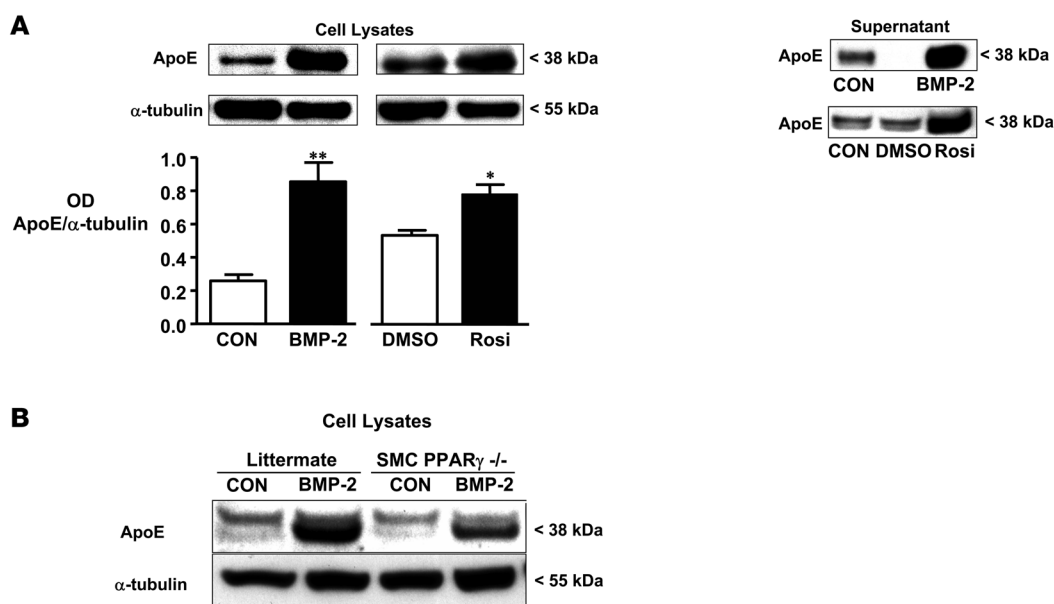


Figure 5

BMP-2 and the PPAR γ agonist rosiglitazone induce apoE in PSMCs. (A) apoE protein expression in cell lysates (left) and apoE protein secretion in supernatant (right) induced by BMP-2 (10 ng/ml, 24 hours) and rosiglitazone (1 μ M, 24 hours) were detected by immunoblotting as described in Methods (for cell lysates, densitometric values were corrected for equal loading using α -tubulin). For apoE secretion, the media of 3–4 cell culture flasks per condition were pooled and concentrated for the blots shown (representative of 2 independent experiments with similar results). (B) BMP-2-induced (10 ng/ml, 24 hours) upregulation of apoE in murine control PSMCs was reduced by half in PSMCs harvested from *SM22 α Cre PPAR γ ^{fllox/fllox}* mice. PSMCs were isolated from 5 littermate control and 5 *SM22 α Cre PPAR γ ^{fllox/fllox}* mice as described in Methods. PSMCs from each genotype were then pooled and subcultured prior to stimulation with BMP-2. The blot is representative of 2 independent experiments with similar results. For apoE protein levels in cell lysates (A), bars represent mean \pm SEM ($n = 3$). * $P < 0.05$; ** $P < 0.01$ versus control; unpaired 2-tailed t test.

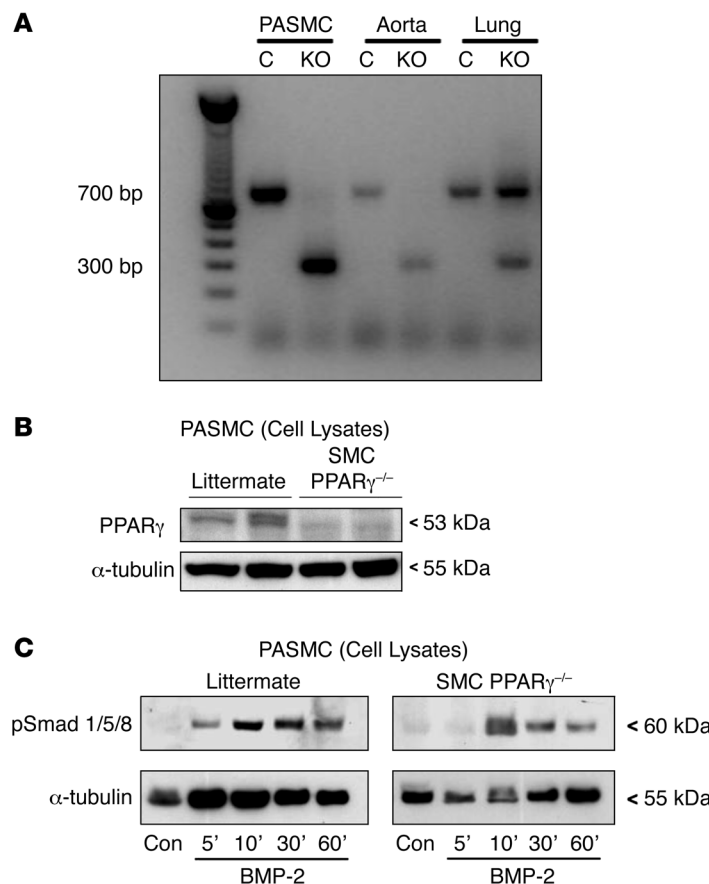


Figure 6

Mice with targeted deletion of PPAR γ in SMCs maintain BMP-2-induced pSmad1/5/8 signaling. **(A and B)** Genotyping of mice with targeted deletion of PPAR γ in SMCs. **(A)** PCR reactions showing gain of a 300-bp knockout transcript and almost complete loss of the 700-bp wild-type transcript in PASM and aorta from *SM22 α Cre PPAR $\gamma^{lox/lox}$* mice. In the lung, which contains SMCs but also many other cell types, both transcripts are found in *SM22 α Cre PPAR $\gamma^{lox/lox}$* mice, whereas only the wild-type transcript is detected in littermate control mice. **(B)** Western immunoblotting of PASM lysates isolated from both littermate and *SM22 α Cre PPAR $\gamma^{lox/lox}$* (SMC PPAR $\gamma^{-/-}$) mice ($n = 2$ each) showed no detectable PPAR γ protein expression when compared with control cells. **(C)** Both littermate control and SMC PPAR $\gamma^{-/-}$ PASM were stimulated with BMP-2 (10 ng/ml) for 5–60 minutes as described in the legend for Figure 1, and phospho-Smad 1/5/8 protein expression was detected by immunoblotting as described in Methods (densitometric values were corrected for equal loading using α -tubulin). Data for 1 of 2 representative experiments with similar results are shown.

tion factor PPAR γ and the growth-promoting MAPK nuclear phospho-ERK (30). We observed that BMP-2 activation of PPAR γ in HPASMCs was independent of the phospho-Smad1/5/8 pathway but correlated with reduced nuclear phospho-ERK expression, presumably due to PPAR γ activation of phosphatases (14, 15) or inhibition of phospho-ERK nuclear translocation (27). Conversely, PDGF-BB/PDGFR- β -mediated induction of nuclear phospho-ERK was associated with reduced PPAR γ DNA binding, probably due to phosphorylation and inactivation of PPAR γ at its N terminus (28) and/or enhancement of nuclear export (31) or ubiquitin/proteasome-mediated degradation and rapid turnover of PPAR γ (32). Thus, it may be that continuous endogenous BMP-2/BMPRII signaling is necessary as a gatekeeper to prevent inactivation of PPAR γ and nuclear translocation of phospho-ERK in response to PDGF-BB/PDGFR- β stimulation.

Low-dose rosiglitazone and a physiological dose of recombinant apoE completely blocked PDGF-BB-induced proliferation of HPASMCs, consistent with previous work in *systemic* SMCs (12, 33). Since we showed that both BMP-2 and rosiglitazone induce apoE protein synthesis and secretion in HPASMCs, we reason that, in addition to lowering phospho-ERK in the nucleus, PPAR γ -mediated induction of apoE inhibits PDGF-BB/PDGFR- β signaling (20, 21). The fact that some upregulation of apoE by BMP-2 occurs even in PPAR γ -deficient SMCs indicates that apoE also can be regulated by a PPAR γ -independent pathway. Further studies using apoE promoter-reporter assays would delineate the nature of PPAR γ -mediated transcriptional activation of this target gene.

The *spontaneous* development of PAH in the *SM22 α Cre PPAR $\gamma^{lox/lox}$* mice is in contrast to our observations that apoE $^{-/-}$ mice at similar age develop PAH only when fed a high-fat diet leading to insulin resistance (25). Since we found that the PPAR γ agonist rosiglitazone can completely reverse PAH in the apoE $^{-/-}$ mouse, multiple other PPAR γ -dependent mechanisms in addition to apoE induction may prevent PASM proliferation and PAH in response to growth factors. In our previous study, we attributed the rescue effect of PPAR γ activation to enhanced production of adiponectin, an adipocytokine that sequesters the ligand PDGF-BB, thereby inhibiting SMC proliferation and survival (34). However, we have not been able to detect adiponectin mRNA or protein expression in HPASMCs. Nonetheless, activated PPAR γ can induce multiple other growth-inhibitory and proapoptotic gene products and repress growth-promoting factors in vascular cells (Figure 8C). For example, PPAR γ activation blocks PDGF gene expression (35) and induces the expression of LRP (36), the receptor necessary for apoE-mediated suppression of PDGF-BB signaling (20, 21) (Figure 8, A and C). PPAR γ activation also reduces levels of endothelin-1 (ET-1) (37) and the endogenous nitric oxide synthase inhibitor asymmetric dimethylarginine (ADMA) (38, 39), factors that are implicated in the pathobiology of PAH (39). Moreover, activated PPAR γ stabilizes the cyclin-dependent kinase inhibitor p27^{KIP1} (40) and inhibits telomerase activity (41), retinoblastoma protein phosphorylation (40), and ultimately G₁ to S phase transition, cell-cycle progression, and vascular SMC proliferation (40). By blocking important survival pathways downstream of activated PDGFR- β , i.e., PI3K (42),

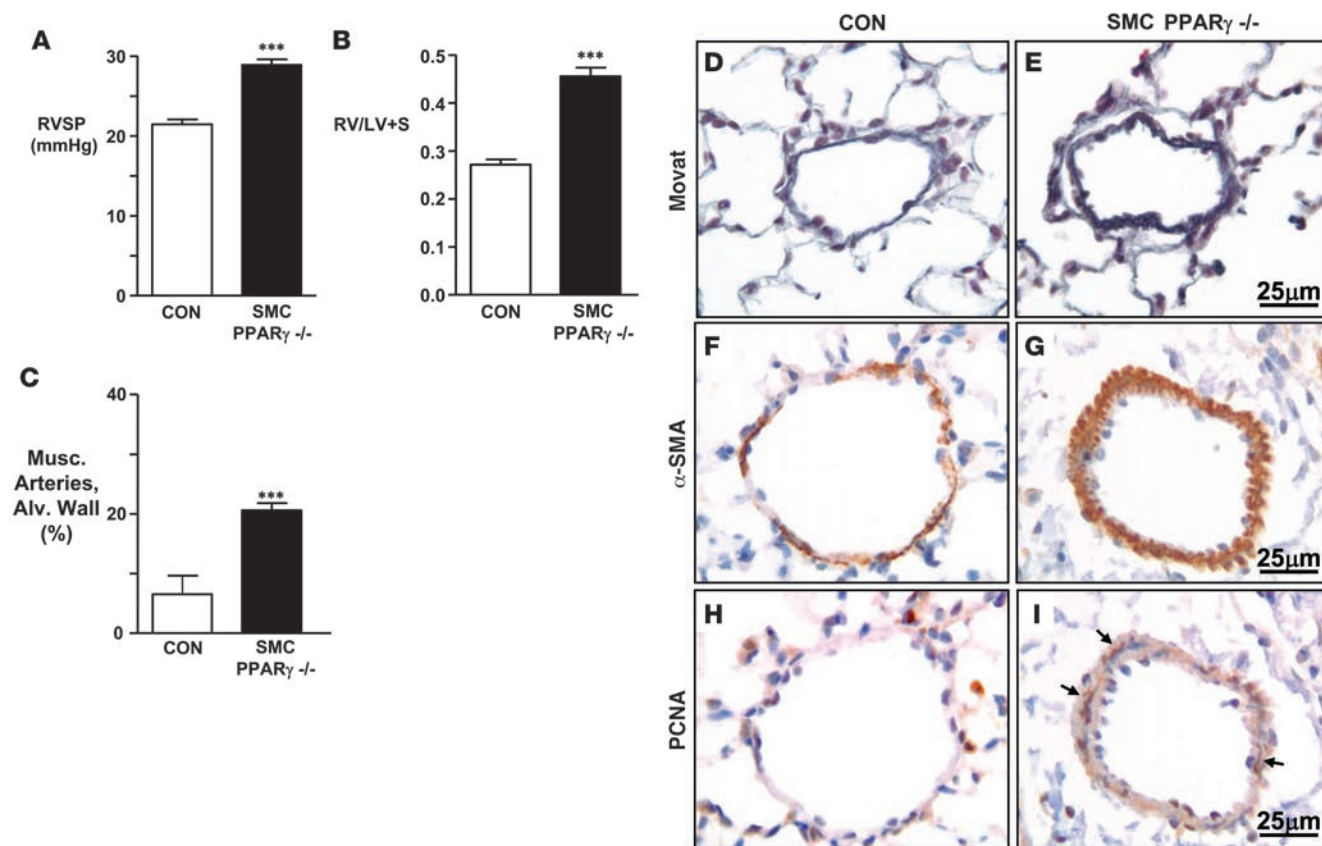


Figure 7

PAH in mice with targeted deletion of PPAR γ in SMCs. Thirteen- to 15-week-old mice underwent RV catheterization, followed by organ harvest. (A) RVSP measurements, as described in Methods. (B) Right ventricular hypertrophy (RVH), measured as ratio of the weight of the RV to that of the LV plus septum (RV/LV+S), as described in Methods. (C) Muscularization of alveolar wall arteries (Musc. Arteries Alv. Wall), as described in Methods. (D) Representative photomicrographs of lung tissue (stained by Movat pentachrome) of 15-week-old mice showing a typical nonmuscular peripheral alveolar artery in a littermate control mouse. (E) A similar section in the SM22 α Cre PPAR $\gamma^{flox/flox}$ (SMC PPAR $\gamma^{-/-}$) mouse shows an alveolar wall artery surrounded by a rim of muscle. (F–I) Immunohistochemistry in serial lung tissue sections from littermate control (CON) and SMC PPAR $\gamma^{-/-}$ mice stained for α -SMA (F and G) and proliferating cell nuclear antigen (PCNA; H and I). Arrows in I indicate enhanced PCNA staining in PASMCs. See also Table 1. Bars represent mean \pm SEM ($n = 5$). *** $P < 0.001$ versus control; unpaired 2-tailed t test.

PPAR γ agonists also lead to apoptosis of proliferating vascular cells (12, 43). In addition, it is known that PPAR γ ligands impair production of matrix metalloproteinases (44) that can be activated by elastase (45). Our group has shown that inhibition of this proteolytic cascade not only prevents but also reverses advanced fatal PAH in rats (46).

Previous studies have shown beneficial effects of BMP-2 (47), PPAR γ activation (reviewed in ref. 12), and apoE (18, 19) in preventing systemic vascular pathology, but our observations are the first indication to our knowledge that all 3 factors are linked. More recently, a connection between PPAR γ and apoE has been made in patients with Alzheimer disease, in that the improvement of cognitive function with rosiglitazone is not apparent in patients who carry the APOE epsilon 4 allele (48). Hence, the novel axis we describe may be relevant in addressing mechanisms that underlie many different pathologic processes.

In summary, our data reveal a novel PPAR γ /apoE axis downstream of BMP-2 signaling in HPASMCs. Failure to activate PPAR γ in response to BMP-2 when there is BMP-RII dysfunction could place a patient at risk for the development or progression of PAH.

We suggest that PPAR γ agonists might rescue BMP-RII dysfunction and reverse SMC proliferation and vascular remodeling in PAH patients and may be useful antiproliferative agents even in those patients without BMP-RII dysfunction.

Methods

Additional and more detailed methods are provided in the supplemental materials.

Creation of mice with targeted deletion of PPAR γ in arterial SMCs using the Cre-loxP system. We cross-bred SM22 α promoter-driven Cre-transgenic mice with PPAR γ homozygous floxed mice. Both strains were obtained from the Jackson Laboratory, and the cross resulted in SM22 α Cre PPAR $\gamma^{flox/flox}$ (SMC PPAR $\gamma^{-/-}$) mice. The offspring genotypes were determined by PCR (see Supplemental Methods). PCR conditions and primer information are available from the Jackson Laboratory. For the experiments involving PASMC isolation and subculture described below, apoE-deficient (B6.129P2-Apoetm1Unc/J) and C57BL/6 control mice were purchased from the Jackson Laboratory.

Genotyping/RT-PCR analysis. To detect the deletion of PPAR γ exon 1 and exon 2, two primers were designed and located in exon A1 and exon

**Table 1**

Invasive hemodynamic, echocardiographic, heart weight, pulmonary artery, hematocrit, wbc, and blood glucose measurements in *SM22α PPAR_γ Cre^{flax/flax}* (SMC PPAR_γ^{-/-}) and littermate control mice

	Littermate control	SMC PPAR _γ ^{-/-}	<i>P</i>	<i>n</i>
Body weight (g)	22.5 ± 0.9	22.1 ± 1.2		8–10
Hemodynamics				
RVSP (mmHg)	21.5 ± 0.6	29.0 ± 0.6	<i>P</i> < 0.001	7–8
RV <i>dP/dt</i> max (mmHg/s)	1,439 ± 144	1,718 ± 143		7–8
RV <i>dP/dt</i> min (mmHg/s)	-1,228 ± 87	-1,405 ± 63		7–8
Systolic BP (mmHg)	105 ± 3.2	97 ± 3.1		9–10
MAP (mmHg)	85 ± 2.0	78 ± 3.1		9–10
Diastolic BP (mmHg)	74 ± 1.9	68 ± 3.1		9–10
Echocardiography				
Heart rate (bpm)	423 ± 22	411 ± 20		9–10
Ejection fraction (%)	72.7 ± 2.2	76.8 ± 1.2		9–10
Fractional shortening (%)	36.5 ± 1.8	39.8 ± 1.1		9–10
Cardiac output (ml/min)	35.3 ± 2.7	38.7 ± 3.6		9–10
LVIDD (mm)	3.58 ± 0.05	3.62 ± 0.10		9–10
LVISD (mm)	2.26 ± 0.09	2.19 ± 0.09		9–10
LVPWd (mm)	0.60 ± 0.04	0.58 ± 0.03		9–10
IVSd (mm)	0.56 ± 0.02	0.55 ± 0.02		9–10
Heart weight				
RV/LV+S	0.26 ± 0.01	0.46 ± 0.02	<i>P</i> < 0.0001	8–10
RV/body weight (×10 ³)	0.88 ± 0.05	1.33 ± 0.05	<i>P</i> < 0.0001	8–10
Number and muscularization of pulmonary arteries				
No. of arteries/alveoli (%)	2.2 ± 0.2	2.3 ± 0.2	<i>P</i> = 0.0014	5–6
Musc. arteries, alv. wall (%)	6.5 ± 3.1	20.6 ± 1.2		5–6
Blood				
HCT (%)	48.7 ± 0.8	49.3 ± 1.0	<i>P</i> = 0.0168	8
wbc count (×10 ³ cells/μl)	5.2 ± 0.8	7.4 ± 0.4		8–10
Glucose (mg/dl)	126.6 ± 6.2	122.8 ± 4.2		9–10

Thirteen- to 15-week-old male littermate control and SMC PPAR_γ^{-/-} mice on regular chow in normoxia. Data are shown as mean ± SEM. Statistically significant differences (P < 0.05; unpaired 2-tailed t test) between genotypes are indicated. dP/dt max., maximal rate of pressure development (systolic RV function); dP/dt min., max. rate of pressure decay (diastolic RV function); MAP, mean arterial pressure; EF, ejection fraction; FS, fractional shortening; LVIDD, LV end-diastolic inner diameter; LVISD, LV end-systolic inner diameter; LVPWd, LV end-diastolic posterior wall thickness; IVSd, end-diastolic interventricular septum thickness; LV+S, LV plus septum; Alv., alveolar; Musc., muscularization; HCT, hematocrit.

4 of the *Pparg1* gene for RT-PCR to recognize the full-length (700 bp) and recombined mRNA (300 bp), as previously described (49) (for primers and PCR protocol, see Supplemental Methods). Total RNA was extracted from PSMCs, aorta, and lung with TRIzol reagent (Invitrogen). PSMCs were obtained from pulmonary arteries of *SM22α Cre PPAR_γflax/flax* mice and littermate control mice and cultured for 10 days. Then RNA samples from the cells were reverse transcribed using the Superscript III Reverse Transcriptase kit (Invitrogen). PCR was applied to cDNA using a Taq DNA polymerase kit (Invitrogen), and transcripts were run on a 1% agarose gel.

Lentiviral shRNAi gene silencing of human BMP-RII. For long-term gene silencing of BMP-RII in HPASMCs, we constructed a pLentivirus 6 with an integrated short hairpin oligonucleotide directed against the mRNA of human BMP-RII, using an inducible H1 RNAi entry vector kit and a lentiviral RNAi expression system kit (K4920-00, K4943-00; Invitrogen) as described by the manufacturer (for details, see Supplemental Methods). Lentivirus was made and propagated in 293FT cells, and HPASMCs were transfected as described in Supplemental Methods. After 12 days of blasticidin selection, we confirmed an 85% stable knockdown of human BMP-RII compared with shLacZi control in HPASMCs (Supplemental Figure 1) and continued with further experiments.

Cell culture. Primary murine PSMCs were isolated from 13- to 15-week-old apoE^{-/-} and C57BL/6 mice, as well as *SM22α Cre PPAR_γflax/flax* and littermate control mice, using a modified elastase/collagenase digestion protocol as previously described (50). Primary HPASMCs were purchased from Cascade Biologics. Moreover, control PSMCs were isolated from surgical resection specimens derived from a patient undergoing lobectomy or pneumonectomy for suspected lung tumor. Additional PSMCs were obtained from a patient undergoing heart-lung transplantation for FPAH and known to harbor a mutation in BMP-RII (W9X), as previously described (51). The nature of the BMP-RII mutation, cell isolation, and culture techniques are described in Supplemental Methods.

Cell proliferation assays. For determination of cell number, PSMCs were seeded at 2.5 × 10⁴ cells per well of a 24-well plate in 500 μl of growth medium and allowed to adhere overnight. The medium was removed and the cells washed 3 times with PBS prior to the addition of starvation media (DMEM, 0.1% FBS, penicillin/streptomycin) and incubated at 37°C, 5% CO₂ for 24 hours (murine PSMCs) or 48 hours (HPASMCs) prior to PDGF-BB stimulation (20 ng/ml) for 72 hours (treatments and concentrations are given in the figure legends). The media with or without growth factors and/or inhibitors was changed every 24 hours. Cells were washed twice with PBS and trypsinized in 150 μl of trypsin/EDTA for 7 minutes, followed by the addi-

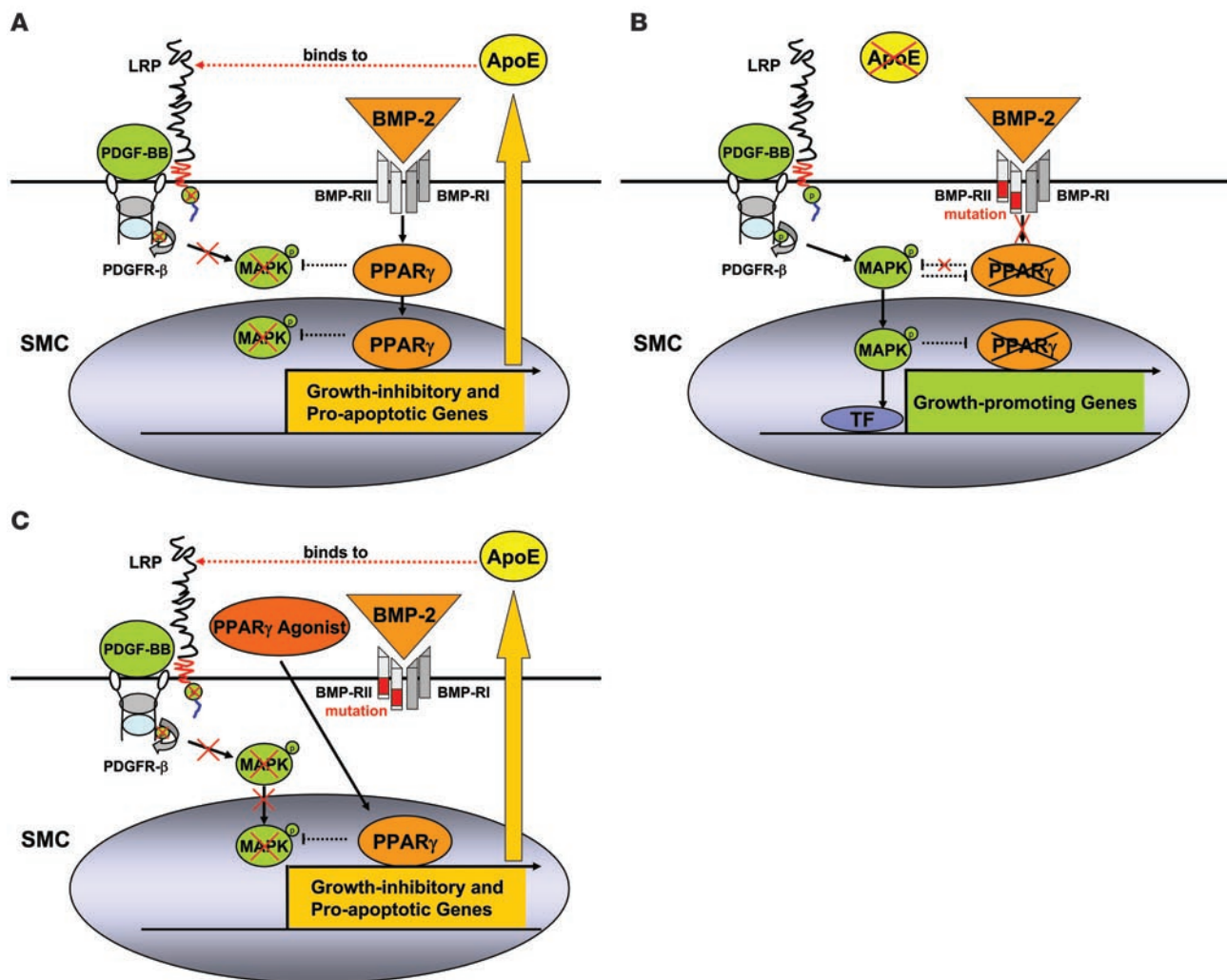


Figure 8

Model: A novel antiproliferative BMP-2/PPAR γ /apoE axis protects against PAH. This schema incorporates the findings described in our article and the literature to date as discussed. **(A)** BMP-2 inhibits SMC proliferation via PPAR γ and apoE. apoE impairs PDGF-BB/MAPK signaling by binding to LDL receptor-related protein (LRP), thereby initiating endocytosis and degradation of the LRP/PDGFR- β /PDGF-B complex. PPAR γ induces LRP and other growth-inhibitory/proapoptotic genes in SMCs and inhibits cell-cycle and other growth-promoting genes such as telomerase, cyclin D1, and retinoblastoma protein. Moreover, PPAR γ induces phosphatases that can directly inactivate phospho-ERK. **(B)** BMP-RII dysfunction promotes SMC proliferation and survival in PAH. Heightened PDGF-BB signaling leading to SMC proliferation is a key clinical feature of PAH. Deficiency of both apoE and LRP enhances mitogenic PDGF-BB/MAPK signaling. Loss-of-function mutations in the BMP-RII gene will decrease endogenous PPAR γ activity, leading to unopposed MAPK signaling, SMC proliferation and survival, and ultimately development of PAH. TF, transcription factor. **(C)** PPAR γ agonists can rescue BMP-RII dysfunction and reverse PAH. PPAR γ agonists such as rosiglitazone or pioglitazone might reverse SMC proliferation and vascular remodeling in PAH patients with or without BMP-RII dysfunction via induction of apoE and other growth-inhibitory/proapoptotic genes (as indicated) and through repression of growth-promoting genes (not shown).

tion of 150 μ l trypsin neutralizer (Cascade Biologics). The cells were then resuspended and counted in a hemacytometer (3–6 wells per condition, 4 counts per well). The biochemical MTT cell proliferation assay (ATCC) is described in Supplemental Methods. In cell proliferation studies, BMP-2 (10 ng/ml; Sigma-Aldrich), rosiglitazone (1 μ M; Alexis), or recombinant human apoE (1–10 μ M; Chemicon) were added to quiescent cells 30 minutes prior to mitogenic stimulation with PDGF-BB (human, 20 ng/ml; R&D Systems) for 72 hours. The PPAR γ antagonist GW9662 (1 μ M; Cayman) was added 24 hours prior to the addition of BMP-2. The media with or without growth factors and/or inhibitors was changed every 24 hours.

Protein expression and compartmental localization. Murine and human PASMCs (wild-type, shLacZi control, or shBMP-RIIi) were grown to 70%

confluence and cultured in starvation media (DMEM, 0.1% FBS, 100 U/ml penicillin, 0.1 mg/ml streptomycin; Gibco; Invitrogen) for 24 and 48 hours, respectively. PDGF-BB, BMP-2, apoE, or rosiglitazone was added to quiescent cells for 5–60 minutes and for 24 hours (treatments and concentrations are stated in the figure legends). In addition to total cell lysates, subcellular fractions (nuclear matrix, nuclear extract, cytoplasmic extract) were prepared using a modified low-salt/high-salt protocol as previously described (52). For details, see Supplemental Methods.

apoE protein secretion. Quiescent HPASMCs were cultured in T75 cell culture flasks (75 cm²) covered with minimal media (1 ml) and were then stimulated with BMP-2 (10 ng/ml) or rosiglitazone (1 μ M) for 24 hours. The supernatant media was collected from 3 cell culture flasks per con-



dition, pooled, and concentrated using an Amicon-4 Centrifuge device (Millipore). Protein extracts were then prepared as described in Supplemental Methods, and 20 µg protein per sample was loaded for SDS-PAGE immunoblotting (Invitrogen).

Western immunoblotting. Preparation of subcellular fractions (nuclear matrix, nuclear extract, cytoplasmic extract) and whole-cell lysates (protein extracts) as well as immunoblotting techniques are described in Supplemental Methods. Primary antibodies against phospho-ERK1/2, ERK 1/2, phospho-Smad1/5/8, Smad1 (all Cell Signaling Technology), PPARγ (Santa Cruz Biotechnology Inc.), apoE (Abcam), BMP-RII (BD Biosciences—Pharmingen), and α-tubulin (Sigma-Aldrich) were used.

PPARγ DNA binding assay. A multiplex transcription factor DNA binding assay (Marligen Biosciences) was performed as previously described (53). Briefly, nuclear extracts were incubated with a mixture of biotinylated DNA probes representing different transcription factor binding sites (e.g., for PPARγ, 5'-TGACCTTTGACCTAGAA-3'), each containing a distinct single-stranded sequence that serves as a capture tag. Following the transcription factor binding reactions, samples were incubated with proprietary reagents to digest any DNA probes not bound to transcription factors. Reactions were then incubated with a mix containing spectrally distinct bead sets, and intact biotinylated probes were captured onto corresponding bead surfaces by capture-tag and anti-tag sequence interactions. Beads were then washed using a filter plate and stained with streptavidin-PE. The fluorescent signal associated with transcription factor binding sites localized on the surface of spectrally distinct beads was measured using Luminex-100 instrumentation. Each reaction was carried out in triplicate, so that 300 different data points per sample were obtained for analysis.

Experimental design for studies in transgenic mice. SM22α Cre PPARγ^{flax/flax} or littermate control mice were maintained on regular chow with free access to drinking water. All studies were carried out in 13- to 15-week-old mice under a protocol approved by the Animal Care Committee of Stanford University following the guidelines of the American Physiological Society.

Hemodynamic measurements. RVSP and RV dp/dt measurements were performed in 15-week-old nonventilated mice under isoflurane anesthesia (1.5%–2.5%, 2 l O₂/min) by inserting a 1.4 F catheter (Millar Instruments) via the right jugular vein as described previously (25). Systemic blood pressure was determined in nonanesthetized, 14- to 15-week-old mice by the tail cuff method using the BP 2000 analysis system (Visitech Systems). Cardiac output and function were measured in 13- to 15-week-old mice by echocardiography under isoflurane anesthesia (1%, 1 l O₂/min) with an ultrasound machine (Vivid 7; GE Medical Systems) using a 13-MHz linear array transducer (see Supplemental Methods).

RVH and LVH. RVH was measured as described previously (54) by the weight of the RV relative to LV plus septum. LVH was measured as absolute weight of the LV plus septum relative to body weight. LV dilatation was assessed by echocardiographic M-mode measurement of the LVIDD.

Lung tissue preparation. Lungs were perfused with normal saline, fixed in 10% formalin overnight, and then embedded in paraffin for routine histology (H&E, elastin van Gieson, Movat pentachrome), as previously described (25, 54). A subset of left lungs (approximately half) were injected with barium-gelatin via pulmonary artery-inserted tubing (25) to label peripheral pulmonary arteries for morphometric analysis (see Supplemental Methods).

Morphometric analysis. Barium-injected, transverse left lung step sections were stained by the elastin van Gieson method. From all mice, we took the same full section in the mid-portion of the barium-injected left

lung parallel to the hilum and embedded it in the same manner. Pulmonary artery muscularization was assessed at ×400 magnification by calculating the proportion of fully and partially muscularized peripheral (alveolar wall) pulmonary arteries to total peripheral pulmonary arteries in 5 random fields (1 field = ×200 magnification). The total number of alveolar wall and duct arteries was expressed as both the ratio of number of pulmonary arteries per 100 alveoli and number of pulmonary arteries per surface area (5 random fields at ×200 magnification). Approximately 1,000 alveoli were counted per animal. All measurements were carried out by investigators blinded to genotype and condition.

Immunohistochemistry. Paraffin-embedded sections were deparaffinized in xylene and rehydrated through graded alcohol. Antigen retrieval was performed using a heat-mediated epitope retrieval method by heating the sections in citrate buffer (10 mM sodium citrate, 0.05% Tween-20, pH 6.0) for 10 minutes at 95°C and then allowing the sections to cool to room temperature. Sections were then incubated with primary antibodies specific for PCNA and α-SMA (Abcam) overnight at 4°C. Staining was then completed using the Vectastain Elite ABC Kit (Vector Laboratories) according to the manufacturer's instructions, using 3,3'-diaminobenzidine as a substrate for peroxidase, and counterstained with hematoxylin.

Fasting whole-blood measurements. Tail vein puncture was performed in nonanesthetized, overnight-starved mice, followed by immediate, duplicate whole-blood glucose measurements with a glucometer (FreeStyle; Abbott), to rule out any influence of the SMC-targeted PPARγ knockout on glucose homeostasis. Additional blood was obtained by cardiac puncture after the hemodynamic measurements. White blood cell count and hematocrit were assessed by the Stanford Animal Facility Laboratories (see Supplemental Methods).

Statistics. Values from multiple experiments are expressed as mean ± SEM. Statistical significance was determined using 1-way ANOVA. When only 2 groups were compared, statistical differences were assessed with the unpaired 2-tailed *t* test. A *P* value of less than 0.05 was considered as significant. The number of samples or animals in each group is indicated in the figure legends.

Acknowledgments

We thank Pete Clausen (Marligen Biosciences) for help with the multiplex DNA binding assay and data analysis. This work was supported by a Postdoctoral Fellowship from the American Heart Association/Pulmonary Hypertension Association (0425943H) to G. Hansmann; the NIH (1-R01-HL074186-01) and the Dwight and Vera Dunlevie Endowed Professorship to M. Rabinovitch; a National Heart, Lung, and Blood Institute National Research Service Award (2-T32-HL007708-14) to J.M. Bekker; and a Predoctoral Fellowship from Boehringer Ingelheim Funds to S. Schellong. N.W. Morrell received grant funding from the British Heart Foundation.

Received for publication April 25, 2007, and accepted in revised form February 6, 2008.

Address correspondence to: Marlene Rabinovitch, Vera Moulton Wall Center for Pulmonary Vascular Disease, Stanford University School of Medicine, CCSR Building, Room 2245B, 269 Campus Drive, Stanford, California 94305-5162, USA. Phone: (650) 723-8239; Fax: (650) 723-6700; E-mail: marlener@stanford.edu.

1. Merklinger, S.L., Jones, P.L., Martinez, E.C., and Rabinovitch, M. 2005. Epidermal growth factor receptor blockade mediates smooth muscle cell apoptosis and improves survival in rats with pulmonary hypertension. *Circulation*. **112**:423–431.

2. Schermuly, R.T., et al. 2005. Reversal of experimental pulmonary hypertension by PDGF inhibition. *J. Clin. Invest.* **115**:2811–2821.

3. Lane, K.B., et al. 2000. Heterozygous germline mutations in BMPR2, encoding a TGF-beta receptor,

cause familial primary pulmonary hypertension. The International PPH Consortium. *Nat. Genet.* **26**:81–84.

4. Deng, Z., et al. 2000. Familial primary pulmonary hypertension (gene PPH1) is caused by mutations



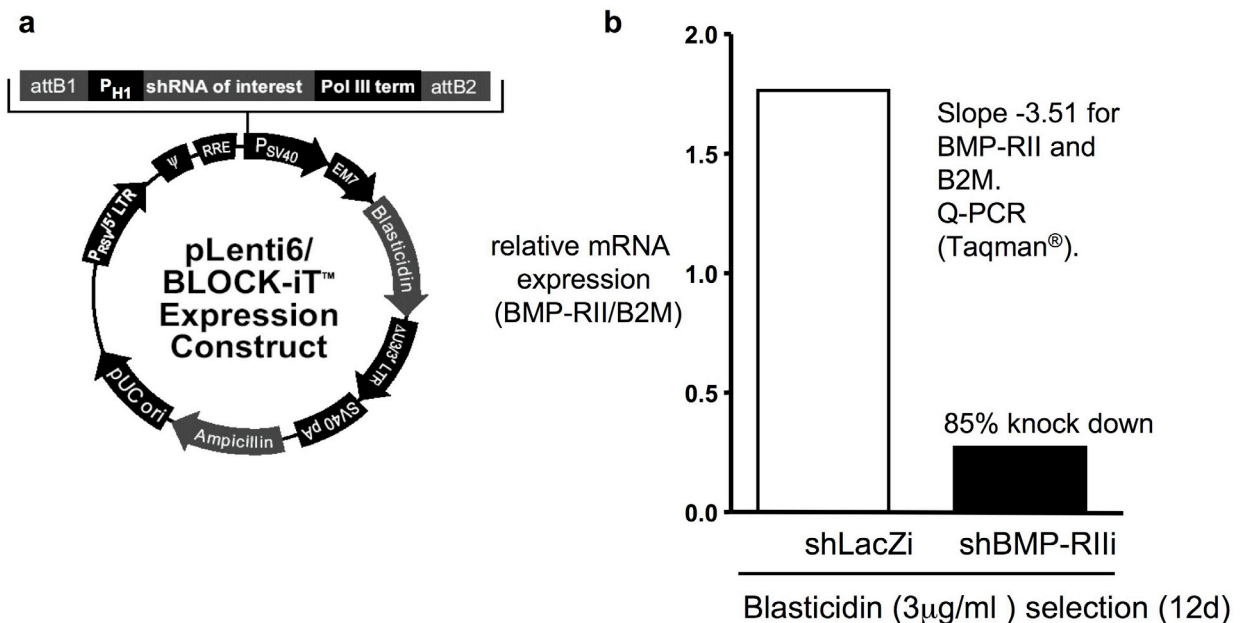
- in the bone morphogenetic protein receptor-II gene. *Am. J. Hum. Genet.* **67**:737–744.
5. Newman, J.H., et al. 2004. Genetic basis of pulmonary arterial hypertension: current understanding and future directions. *J. Am. Coll. Cardiol.* **43**:33S–39S.
6. Humbert, M., et al. 2002. BMPR2 germline mutations in pulmonary hypertension associated with fenfluramine derivatives. *Eur. Respir. J.* **20**:518–523.
7. Roberts, K.E., et al. 2004. BMPR2 mutations in pulmonary arterial hypertension with congenital heart disease. *Eur. Respir. J.* **24**:371–374.
8. Atkinson, C., et al. 2002. Primary pulmonary hypertension is associated with reduced pulmonary vascular expression of type II bone morphogenetic protein receptor. *Circulation.* **105**:1672–1678.
9. Galetto, R., et al. 2001. Identification of a peroxisome-proliferator-activated-receptor response element in the apolipoprotein E gene control region. *Biochem. J.* **357**:521–527.
10. Ameshima, S., et al. 2003. Peroxisome proliferator-activated receptor gamma (PPARgamma) expression is decreased in pulmonary hypertension and affects endothelial cell growth. *Circ. Res.* **92**:1162–1169.
11. Geraci, M.W., et al. 2001. Gene expression patterns in the lungs of patients with primary pulmonary hypertension: a gene microarray analysis. *Circ. Res.* **88**:555–562.
12. Marx, N.N., Duez, H.H., Fruchart, J.C., and Staels, B. 2006. Peroxisome proliferator-activated receptors and atherogenesis: regulators of gene expression in vascular cells. *Circ. Res.* **94**:1168–1178.
13. Gilde, A.J., Fruchart, J.C., and Staels, B. 2006. Peroxisome proliferator-activated receptors at the crossroads of obesity, diabetes, and cardiovascular disease. *J. Am. Coll. Cardiol.* **48**:A24–A32.
14. Benkirane, K., Amiri, F., Diep, Q.N., El Mabrouk, M., and Schiffrin, E.L. 2006. PPAR-gamma inhibits ANG II-induced cell growth via SHIP2 and 4E-BP1. *Am. J. Physiol. Heart Circ. Physiol.* **290**:H390–H397.
15. Wakino, S., et al. 2001. Peroxisome proliferator-activated receptor gamma ligands inhibit mitogenic induction of p21(Cip1) by modulating the protein kinase Cdelta pathway in vascular smooth muscle cells. *J. Biol. Chem.* **276**:47650–47657.
16. Akiyama, T.E., et al. 2002. Conditional disruption of the peroxisome proliferator-activated receptor gamma gene in mice results in lowered expression of ABCA1, ABCG1, and apoE in macrophages and reduced cholesterol efflux. *Mol. Cell. Biol.* **22**:2607–2619.
17. Yue, L., Rasouli, N., Ranganathan, G., Kern, P.A., and Mazonne, T. 2004. Divergent effects of peroxisome proliferator-activated receptor gamma agonists and tumor necrosis factor alpha on adipocyte ApoE expression. *J. Biol. Chem.* **279**:47626–47632.
18. Zeleny, M., Swertfeger, D.K., Weisgraber, K.H., and Hui, D.Y. 2002. Distinct apolipoprotein E isoform preference for inhibition of smooth muscle cell migration and proliferation. *Biochemistry.* **41**:11820–11823.
19. Ishigami, M., Swertfeger, D.K., Granholm, N.A., and Hui, D.Y. 1998. Apolipoprotein E inhibits platelet-derived growth factor-induced vascular smooth muscle cell migration and proliferation by suppressing signal transduction and preventing cell entry to G1 phase. *J. Biol. Chem.* **273**:20156–20161.
20. Boucher, P., Gotthardt, M., Li, W.P., Anderson, R.G., and Herz, J. 2003. LRP: role in vascular wall integrity and protection from atherosclerosis. *Science.* **300**:329–332.
21. Newton, C.S., et al. 2005. Platelet-derived growth factor receptor-beta (PDGFR-beta) activation promotes its association with the low density lipoprotein receptor-related protein (LRP). Evidence for co-receptor function. *J. Biol. Chem.* **280**:27872–27878.
22. Lassila, M., et al. 2004. Imatinib attenuates diabetes-associated atherosclerosis. *Arterioscler. Thromb. Vasc. Biol.* **24**:935–942.
23. Humbert, M., et al. 1998. Platelet-derived growth factor expression in primary pulmonary hypertension: comparison of HIV seropositive and HIV seronegative patients. *Eur. Respir. J.* **11**:554–559.
24. Ghofrani, H.A., Seeger, W., and Grimminger, F. 2005. Imatinib for the treatment of pulmonary arterial hypertension. *N. Engl. J. Med.* **353**:1412–1413.
25. Hansmann, G., et al. 2007. Pulmonary arterial hypertension is linked to insulin resistance and reversed by peroxisome proliferator-activated receptor-gamma activation. *Circulation.* **115**:1275–1284.
26. Ghosh, S.S., et al. 2003. PPARgamma ligand attenuates PDGF-induced mesangial cell proliferation: role of MAP kinase. *Kidney Int.* **64**:52–62.
27. Goetze, S., et al. 2001. Peroxisome proliferator-activated receptor-gamma ligands inhibit nuclear but not cytosolic extracellular signal-regulated kinase/mitogen-activated protein kinase-regulated steps in vascular smooth muscle cell migration. *J. Cardiovasc. Pharmacol.* **38**:909–921.
28. Hu, E., Kim, J.B., Sarraf, P., and Spiegelman, B.M. 1996. Inhibition of adipogenesis through MAP kinase-mediated phosphorylation of PPARgamma. *Science.* **274**:2100–2103.
29. Ishihara, K., Tsutsumi, K., Kawane, S., Nakajima, M., and Kasaoka, T. 2003. The receptor for advanced glycation end-products (RAGE) directly binds to ERK by a D-domain-like docking site. *FEBS Lett.* **550**:107–113.
30. Sarjeant, J.M., et al. 2003. Apolipoprotein D inhibits platelet-derived growth factor-BB-induced vascular smooth muscle cell proliferation by preventing translocation of phosphorylated extracellular signal regulated kinase 1/2 to the nucleus. *Arterioscler. Thromb. Vasc. Biol.* **23**:2172–2177.
31. Burgermeister, E., et al. 2007. Interaction with MEK causes nuclear export and downregulation of peroxisome proliferator-activated receptor gamma. *Mol. Cell. Biol.* **27**:803–817.
32. Floyd, Z.E., and Stephens, J.M. 2002. Interferon-gamma-mediated activation and ubiquitin-proteasome-dependent degradation of PPARgamma in adipocytes. *J. Biol. Chem.* **277**:4062–4068.
33. Ishigami, M., et al. 2000. Apolipoprotein E inhibition of vascular smooth muscle cell proliferation but not the inhibition of migration is mediated through activation of inducible nitric oxide synthase. *Arterioscler. Thromb. Vasc. Biol.* **20**:1020–1026.
34. Arita, Y., et al. 2002. Adipocyte-derived plasma protein adiponectin acts as a platelet-derived growth factor-BB-binding protein and regulates growth factor-induced common postreceptor signal in vascular smooth muscle cell. *Circulation.* **105**:2893–2898.
35. Zhang, J., Fu, M., Zhao, L., and Chen, Y.E. 2002. 15-Deoxy-prostaglandin J(2) inhibits PDGF-A and -B chain expression in human vascular endothelial cells independent of PPAR gamma. *Biochem. Biophys. Res. Commun.* **298**:128–132.
36. Gauthier, A., Vassiliou, G., Benoist, F., and McPherson, R. 2003. Adipocyte low density lipoprotein receptor-related protein gene expression and function is regulated by peroxisome proliferator-activated receptor gamma. *J. Biol. Chem.* **278**:11945–11953.
37. Martin-Nizard, F., et al. 2002. Peroxisome proliferator-activated receptor activators inhibit oxidized low-density lipoprotein-induced endothelin-1 secretion in endothelial cells. *J. Cardiovasc. Pharmacol.* **40**:822–831.
38. Wakino, S., et al. 2005. Pioglitazone lowers systemic asymmetric dimethylarginine by inducing dimethylarginine dimethylaminohydrolase in rats. *Hypertens. Res.* **28**:255–262.
39. Kielstein, J.T., et al. 2005. Asymmetrical dimethylarginine in idiopathic pulmonary arterial hypertension. *Arterioscler. Thromb. Vasc. Biol.* **25**:1414–1418.
40. Wakino, S., et al. 2000. Peroxisome proliferator-activated receptor gamma ligands inhibit retinoblastoma phosphorylation and G1-> S transition in vascular smooth muscle cells. *J. Biol. Chem.* **275**:22435–22441.
41. Ogawa, D., et al. 2006. Activation of peroxisome proliferator-activated receptor gamma suppresses telomerase activity in vascular smooth muscle cells. *Circ. Res.* **98**:e50–e59.
42. Vantler, M., Caglayan, E., Zimmermann, W.H., Baumer, A.T., and Rosenkranz, S. 2005. Systematic evaluation of anti-apoptotic growth factor signaling in vascular smooth muscle cells. Only phosphatidylinositol 3'-kinase is important. *J. Biol. Chem.* **280**:14168–14176.
43. Brummmer, D., et al. 2003. Regulation of the growth arrest and DNA damage-inducible gene 45 (GADD45) by peroxisome proliferator-activated receptor gamma in vascular smooth muscle cells. *Circ. Res.* **93**:e38–e47.
44. Worley, J.R., et al. 2003. Metalloproteinase expression in PMA-stimulated THP-1 cells. Effects of peroxisome proliferator-activated receptor-gamma (PPAR gamma) agonists and 9-cis-retinoic acid. *J. Biol. Chem.* **278**:51340–51346.
45. Nagase, H., Englund, J.J., Suzuki, K., and Salvesen, G. 1990. Stepwise activation mechanisms of the precursor of matrix metalloproteinase 3 (stromelysin) by proteinases and (4-aminophenyl)mercuric acetate. *Biochemistry.* **29**:5783–5789.
46. Cowan, K.N., et al. 2000. Complete reversal of fatal pulmonary hypertension in rats by a serine elastase inhibitor. *Nat. Med.* **6**:698–702.
47. Nakaoka, T., et al. 1997. Inhibition of rat vascular smooth muscle proliferation in vitro and in vivo by bone morphogenetic protein-2. *J. Clin. Invest.* **100**:2824–2832.
48. Risner, M.E., et al. 2006. Efficacy of rosiglitazone in a genetically defined population with mild-to-moderate Alzheimer's disease. *Pharmacogenomics J.* **6**:246–254.
49. Hevener, A.L., et al. 2003. Muscle-specific Pparg deletion causes insulin resistance. *Nat. Med.* **9**:1491–1497.
50. Fouty, B.W., et al. 2001. p27(Kip1) is important in modulating pulmonary artery smooth muscle cell proliferation. *Am. J. Respir. Cell Mol. Biol.* **25**:652–658.
51. Yang, X., Lee, P.J., Long, L., Trembath, R.C., and Morrell, N.W. 2007. BMP4 induces HO-1 via a Smad-independent, p38MAPK-dependent pathway in pulmonary artery myocytes. *Am. J. Respir. Cell Mol. Biol.* **37**:598–605.
52. Mitani, Y., Zaidi, S.H., Dufourcq, P., Thompson, K., and Rabinovitch, M. 2000. Nitric oxide reduces vascular smooth muscle cell elastase activity through cGMP-mediated suppression of ERK phosphorylation and AML1B nuclear partitioning. *FASEB J.* **14**:805–814.
53. Shurin, G.V., et al. 2005. Loss of new chemokine CXCL14 in tumor tissue is associated with low infiltration by dendritic cells (DC), while restoration of human CXCL14 expression in tumor cells causes attraction of DC both in vitro and in vivo. *J. Immunol.* **174**:5490–5498.
54. Zaidi, S.H., You, X.M., Ciura, S., Husain, M., and Rabinovitch, M. 2002. Overexpression of the serine elastase inhibitor elafin protects transgenic mice from hypoxic pulmonary hypertension. *Circulation.* **105**:516–521.

SUPPLEMENTARY METHODS

Mice Genotyping/RT-PCR Analysis. To detect the deletion of PPAR γ exon 1 and exon 2, two primers (5'-primer: gtcacgttctgacaggactgtgtgac; 3'-primer: tatcactggagatctccgccaacagc) were designed to correspond to exon A1 and exon 4 of the PPAR γ 1 gene. RT-PCR could then be carried out to detect the full length 700bp transcript or the 300bp transcript containing the deletion as previously described (1). Total RNA was extracted from PASMC, aorta and lung with Trizol reagent (Invitrogen, Cat. # 15596-026). PASMC were obtained from pulmonary arteries of *SM22 α Cre PPAR $\gamma^{lox/lox}$* mice (*SMC PPAR γ -/-*) and littermate control mice after 10 days in cell culture (5 mice per genotype and experiment). 3 μ g total RNA (1 μ g from aorta) was treated with DNase I for 30 min at 37°C (Invitrogen, Cat# 18047019) followed by heating at 70°C for 15min (DNase I inactivation). After confirming appropriate RNA quality, RNA samples were subsequently reverse-transcribed (RT) by using the Superscript III reverse transcriptase kit (Invitrogen, Cat# 18080-044). 2 μ g RNA (0.5 from aorta) from each sample was incubated with 1 μ l Oligo dT at 70°C for 10min and then put on ice. Samples were then incubated with 1xRT buffer, 1 μ l of 0.1M DTT, 1 μ l of 10 μ M dNTPs, and 1 μ l of Superscript III in a total 20 μ l volume at 50°C for 1 hour. RT was stopped by heating samples at 70°C for 15 min. After incubating the samples for 20 min. with 1 μ l of RNase H at 37°C, the cDNA was subjected to the PCR reaction using Taq DNA polymerase kit (Invitrogen, Cat#10342-020). 5 μ l of RT product from each sample was used to mix with 3 μ l of 10 x buffer, 1 μ l of 50 mM MgCl₂, 0.5 μ l of 10mM dNTPs, 1 μ l of each primer(20 μ M) and 1 μ l of Taq DNA polymerase in a total 30 μ l volume. Hot start PCR reaction was used at 94°C for 3 min., followed by 35 cycles of 94°C 30 sec, 65°C 30 sec, 72°C 1min. and then 72°C 10min. incubation. PCR products were then run on a 1% agarose gel.

Lentiviral small hairpin RNAi gene silencing (shRNAi against human BMP-RII): For longterm gene silencing of human BMP-RII, we constructed a pLentivirus 6 with an integrated small hairpin oligonucleotide (bottom 5' to 3': (DNA) - AAA AGC AGA TGG ACG CAT GGA ATA TTT CGA TAT TCC ATG CGT CCA TCT GC; top 5' to 3': (DNA) – AAA AGG ACA ATA TTA TGC TCG AAA GTT CGC TTT CGA GCA TAA TAT TGT CC) directed against the mRNA of human BMP-RII, using an inducible H1 RNAi entry vector kit (Invitrogen #K4920-00). Lentivirus was made and propagated with a lentiviral RNAi expression system kit (Invitrogen, #K4943-00), by transfecting 293FT cells with the shRNA-H1-TO-human BMP-RII pLenti6 construct using Lipofectamine 2000 (Invitrogen) and Vira Power Packaging Mix (Invitrogen, #K4944-00) according to the manufacturer's instructions. Virus-containing supernatants were harvested 48 and 72h posttransfection, ultra-filtered (Milipore, centricon Plus-70), and titrated on HT1080 cells (ATCC). A multiplicity of infection (MOI) of one was used for transfection of human PASMC (Cascade biologics, Portland, OR) with shBMP-RII pLenti6 (see [Supplementary Figure 1](#) online) following the manufacturer's instructions: Cells were incubated with virus mix and polybrene (8 μ g/ml) for 6h, and then changed to full growth-medium. Forty-eight hours after the beginning of transfection, blasticidin (3 μ g/ml) was added to Medium 231 medium including 100U/ml Penicillin, 0.1mg/ml streptomycin and smooth muscle growth supplement (SMGS, Cascade Biologics, Portland, OR). A kill curve for blasticidin had been performed on HPASMC and revealed cell death in untransfected HPASMC by day 5 of blasticidin incubation (3 μ g/ml). By day 12 of blasticidin selection, we confirmed by q-PCR a 85% stable knock down of BMP-RII in shBMP-RIIi vs. shLacZi (control) transfected HPASMC.

Construction of pLenti6 H1 with integrated small hairpin vs. Human BMP-RII



Supplementary Figure 1 a, Construction of a pLentivirus 6 (pLenti 6) with integrated small hairpin oligonucleotide vs. human bone morphogenetic protein receptor II (shBMP-RiIi). For longterm gene silencing of human BMP-RII, we constructed a pLentivirus 6 with an integrated small hairpin oligonucleotide (for details see [Supplementary Methods](#) below) directed against the mRNA of human BMP-RII, using an inducible H1 RNAi entry vector kit and lentiviral RNAi expression system kit (Invitrogen #K4920-00, #K4943-00). **b**, Lentivirus was made and propagated in 293FT cells and human PASCs were transfected as described in the [Supplementary Methods](#) below. After 12 days blasticidin selection, we confirmed a 85% stable knock down of human BMP-RII vs. shLacZi control in human PASCs.

attB1, attB2: DNA recombination sequences that permit recombinational cloning of the gene of interest from a Gateway® entry clone (Invitrogen). **P_{H1}**, human H1 promotor: Expression of the shRNA of interest from pENTR™/H1/TO (or a suitable destination vector following LR

recombination) is controlled by the human H1 promoter. The endogenous human H1 promoter normally controls expression of H1 RNA, the RNA component of human RNase P involved in tRNA processing. This particular promoter to control vector-based expression of shRNA molecules in mammalian cells was chosen for the following reasons: 1.) The promoter is recognized by RNA Polymerase III and controls high-level, constitutive expression of shRNA. 2.) The promoter is active in most mammalian cell types. 3.) The promoter is a type III Pol III promoter in that all elements required to control expression of the shRNA are located upstream of the transcription start site. **Pol III term**, RNA polymerase III. **P_{SV40}**, SV40 early promoter and origin: Allows high-level expression of the selection marker and episomal replication in cells expressing the SV40 large T antigen. **EM7** promoter: synthetic prokaryotic promoter for expression of the selection marker in *E. coli*. **Blasticidin resistance gene**: permits selection of stably transduced mammalian cell lines. **Δ U3/HIV-1 truncated 3' LTR**: Allows viral packaging but self-inactivates the 5' LTR for biosafety purposes. The element also contains a polyadenylation signal for transcription termination and polyadenylation of mRNA in transduced cells. **SV40 pA**, SV40 polyadenylation signal. **Ampicillin resistance gene** (β -lactamase): allows selection of the plasmid in *E. coli*. **pUC ori**: permits high-copy replication and maintenance in *E. coli*. **P_{RSV}/5' LTR**, Rous Sarcoma Virus (RSV) enhancer/promoter: Allows Tat-independent production of viral mRNA. HIV-1 truncated 5' LTR: Permits viral packaging and reverse transcription of the viral mRNA. Ψ , HIV-1 psi (ψ) packaging signal: Allows viral packaging. **RRE**, HIV-1 Rev response element (RRE): Permits Rev-dependent nuclear export of unspliced viral mRNA.

Small interfering (si) RNA gene silencing of human BMP-RII. To achieve effective gene knockdown, siRNA duplexes specific for BMP-RII (Dharmacon on-target plus; accession number NM_001204) were transfected into human PSMCs using Lipofectamine 2000 (Invitrogen) following the manufacturer's protocol. Knockdown efficiency was evaluated 48

hours later by measuring protein levels in cell lysates via immunoblotting. Transfection of nontargeting siRNA duplexes (siCONTROL, Dharmacon, Inc) was performed simultaneously to serve as control in all experiments.

Cell Culture and Functional Assays: *Primary murine PASMC* were isolated from 5 male 14-15-week old mice of apoE deficient (apoE $-/-$) and C57Bl/6 mice, as well as *SM22 α Cre PPAR γ flox/flox* (SMC PPAR γ $-/-$) mice and littermate control mice, using a modified protocol as previously described (2): The main extralobular pulmonary arteries were dissected, cleaned from adherent tissue, cut in small pieces and digested for 90 min. in dispersion media containing 0.53mg/ml elastase (Roche), 0.53mg/ml collagenase II (Worthington), 2 mg/ml albumin (Sigma), 0.2mg/ml soybean trypsin inhibitor (Worthington), 40 μ M CaCl $_2$, in HBSS buffer (Gibco). PASMCs were then cultured in DMEM (Gibco) containing FBS (20% for 3 days, then reduced to 10%), 2mM L-glutamine and 100U/ml Penicillin, 0.1mg/ml streptomycin. Passages 3-4 were used for further studies. Smooth muscle cell identity was verified by positive immunohistochemistry staining for SM α -actin (Sigma Aldrich, St. Louis, MO) (>95% of cells stained positive for SM α -actin). PASMC were grown to 70% confluence in DMEM and then cultured for 24h in starvation media (DMEM, 0.1% FBS, 2mM L-glutamine, 100U/ml Penicillin, 0.1mg/ml streptomycin).

Primary human PASMC were purchased from Cascade Biologics (Portland, OR) and maintained cell culture flasks (25-150cm 2) containing Medium 231, Smooth Muscle Growth Supplement (SMGS), 100U/ml penicillin G, 0.1mg/ml Streptomycin sulfate, and 0.25 μ g/ml Amphotericin B (PSA Solution) (all Cascade Biologics). Cells were received at passage 3 and used between passages 5 and 9. Moreover, normal PASMC were isolated from surgical resection specimens derived from patients undergoing lobectomy or pneumonectomy for suspected lung tumor (control). Only uninvolved tissue was used. PASMC were explanted peripheral pulmonary arteries (<1-2mm external diameters, as previously described (3, 4). Cells were maintained in 10% FBS/DMEM and used for experiments between passages 4 and 6.

Additional PASMC were obtained from a patient undergoing heart-lung transplantation for familial PAH and known to harbor a mutation in the BMP-RII receptor. The isolate used was obtained from a patient in which a premature stop codon is inserted in place of tryptophan at position of the amino acid sequence (W9X). The smooth muscle phenotype of isolated cells was confirmed by positive immunofluorescence with antibodies to anti- α -smooth muscle actin antibody (IA4) and anti-smooth muscle specific myosin (hsm-v), as described(6).

Cell Counts: PASMC were seeded at 2.5×10^4 cells per well of a 24-well plate in 500 μ l of growth medium and allowed to adhere overnight. The medium was removed and the cells washed 3 times with PBS prior to the addition of starvation media (DMEM, 0.1% FBS, penicillin/streptomycin) and incubated at 37°C, 5% CO₂ for 24h (murine PASMC) or 48h (human PASMC) prior to PDGF-BB stimulation for 0h and 72h (treatments and concentrations stated in the figure legends). Cells were washed twice with PBS and trypsinized in 150 μ l of Trypsin/EDTA for 7min., followed by the addition of 150 μ l trypsin neutralizer (all Cascade Biologics, Portland, OR). The cells were then resuspended and counted in a hemacytometer (3-6 wells per condition, 4 counts per well).

MTT Cell Proliferation Assay (ATCC, Manassas, VA): 3×10^3 HPASMC per well were seeded and allowed to adhere on a 96-well plate overnight. After removal of the medium, the cells were washed 3 times with PBS prior to the addition of Opti-MEM I (Gibco, Gaithersburg, MD) containing 0.1% FBS, penicillin/streptomycin, and incubated at 37°C, 5% CO₂ for 48h prior to stimulation. The cells were stimulated with PDGF-BB (20ng/ml) for 72h and then incubated with the yellow MTT (3-(4, 5-dimethylthiazolyl)-2, 5-diphenyltetrazolium bromide) for 6h at 37°C, followed by the addition of detergent (room temperature, stored overnight in the dark). The absorbance was measured in a microtiter plate reader (Biorad, Hercules, CA) at 570nm the next day.

Western immunoblotting. *Preparation of total cell lysates.* PASMC were washed three times with ice-cold PBS. Cell lysates were prepared by adding boiling lysis buffer (10mM Tris HCl, 1% SDS, PMSF 0.2mM, protease and phosphatase inhibitor cocktails (Sigma-Aldrich, St. Louis, MO), phosphatase inhibitors cocktails #1 and #2) to the cells, scraping into a 1.5ml microcentrifuge tube and boiling for 10min. prior to centrifugation. The supernatants were transferred to fresh microcentrifuge tubes and stored – 80°C.

Preparation of subcellular fractions (nuclear matrix, nuclear extract, cytoplasmic extract) were performed using a modified low-salt-high-salt-protocol as previously described (7, 8). HPASMC were washed and then scraped in ice-cold PBS. After centrifugation (1850g, 10min., 4°C), the cell pellet was washed again in PBS. After spin down, the cells were then lysed by resuspension in hypotonic buffer (HEPES 10mM, MgCl₂ x 6 H₂O 1.5mM, KCl 19mM, PMSF 0.2mM, DTT 0.5mM), cell swelling on ice for 20min., followed by 15 strokes with a Dounce homogenizer (B pestle). Nuclei were then pelleted at 3300g for 15min., 4°C. *For cytoplasmic extract preparation*, 0.11 vol. of 10X cytoplasmatic extract buffer (HEPES 300mM, MgCl₂ x 6 H₂O 30mM, NaCl 1.4M) was added to the supernatant. After high speed centrifugation at 20,000g for 30min. at 4°C, the supernatant was designated as cytoplasmic extract and stored at – 80°C. *For nuclear extract preparation*, 1/2 packed nuclear volume of high salt buffer (HEPES 20mM, MgCl₂ x 6 H₂O 1.5mM, NaCl 800mM, glycerol 25%, EDTA-Na 0.2mM, PMSF 0.2mM, DTT 0.5mM) was added dropwise to the nuclear pellet, vortexed for 40min. at 4°C., then centrifuged at 20,000g for 30min. at 4°C. The resulting supernatant was designated as nuclear extract and stored at – 80°C. *For nuclear matrix extract preparation*, 1/2 packed nuclear volume (pnv) of high salt buffer was added. The pellet was boiled for 10min, and the nuclear matrix fraction was extracted by vortexing in 2x packed nuclear volume (pnv) SDS buffer for 60min. at 20°C. After centrifugation at 20,000g for 30min., 4°C, the salt resistant supernatant was designated as

nuclear matrix fraction and stored at – 80°C. All buffers contained protease and phosphatase inhibitors (Sigma-Aldrich, phosphatase inhibitor cocktails #1 and #2).

Protein concentration was determined by the Lowry protein assay (Biorad, Hercules, CA). Equal amounts of protein were loaded onto each lane of a 4-12% Bis-Tris gel and subjected to electrophoresis under reducing conditions. After blotting, PVDF-membranes (Invitrogen, Carlsbad, CA) were blocked for 1h (milkpowder 5% in TBS/tween 0.1-0.2%) and incubated with rabbit polyclonal antibodies raised against ERK 1/2 (Cell Signaling, Danvers, MA), , pSmad 1/5/8 or total Smad1 (both Cell Signaling, Danvers, MA), or mouse monoclonal antibodies against phosphoERK 1/2 (Cell Signaling), PPAR γ (Santa Cruz, Santa Cruz, CA), apolipoprotein E (Abcam, Cambridge, MA) or BMP-RII (BD Biosciences Pharmingen, San Jose, CA). Binding of secondary HRP-antibodies were visualized by ECL or ECL plus chemiluminescent (Amersham, Princeton, NJ). Normalization for total cell protein was performed by re-probing the membrane with a mouse monoclonal antibody against α -tubulin (Sigma-Aldrich, St. Louis, MO). Normalization for total protein in cell fractions was achieved by correcting for Ponceau S stain.

PPAR γ -DNA-Binding Assay. A multiplex transcription factor (TF) assay (Marligen Biosciences, Ijamsville, MD) was performed as previously described (9, 10). Briefly, multiple biotin labeled TF DNA probes (DNA multiplex probe mix) are mixed with one nuclear extract protein sample to allow transcription factor-DNA binding. In the following digestion step, DNA sequences that are not bound (and “protected”) by specific transcription factors are destroyed by proprietary reagents. A mix of colored beads (1000 of each color per specific transcription factor) with attached DNA-oligonucleotides complimentary to a sequence in the specific TF DNA probes is added to the tube. Then, DNA binding sites hybridize to their respective beads (PPAR γ core binding site: 5'-TGACCTTTGACC-3') and the entire sample is measured in a Luminex-100 instrumentation (Luminex, Houston, TX) that reads at least 100 signals per

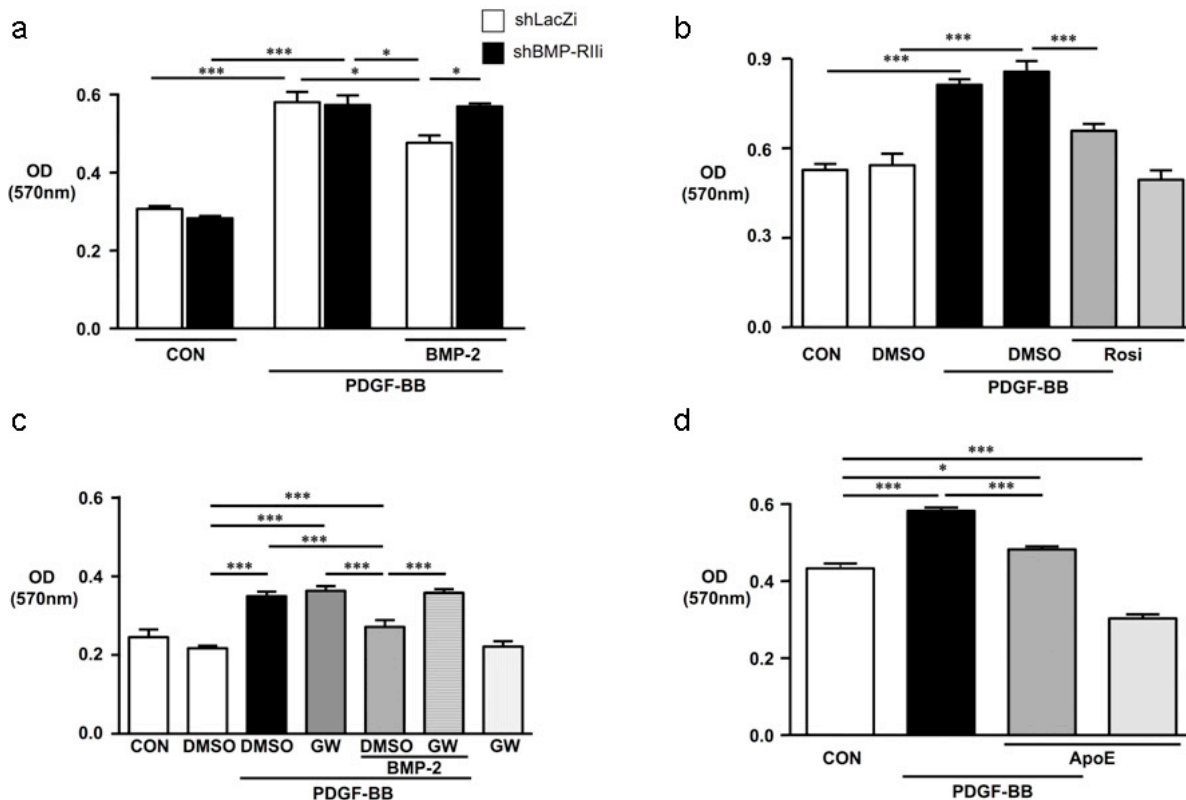
colored bead type. Nuclear extract samples were run in triplicate so that 300 different data points are collected for each DNA binding site.

Immunohistochemistry/Confocal Microscopy. Serum starved Human PASMC were seeded on 4-chamber slides (250 μ l), stimulated with BMP-2 (10ng/ml), washed and fixated with paraformaldehyde 4% at room temperature, incubated in blocking buffer (5% goat serum, 0.02% BSA, Triton X-100 0.1% in TBS) for 30min., and then incubated with primary polyclonal antibody (rabbit anti human) against phosphoERK1/2 (Cell Signalling, Danvers, MA) overnight at 4°C. The fixed cells were then carefully washed three times, and incubated with secondary antibody (goat anti rabbit, Alexa 488, Molecular Probes/Invitrogen, Carlsbad, CA), and again washed three times. For mounting, antifade-DAPI (Component A, slow fade-antifade kit S-24635, Mol. Probes/Invitrogen) was given on the cover slips, and slides were sealed with colorless nail polish. Images were acquired on a Zeiss LSM 510 two-photon confocal laser scanning microscope. Confocal micrographs were processed with Openlab 3.1.4 and Volocity 3.0 software (Improvision, Coventry, UK).

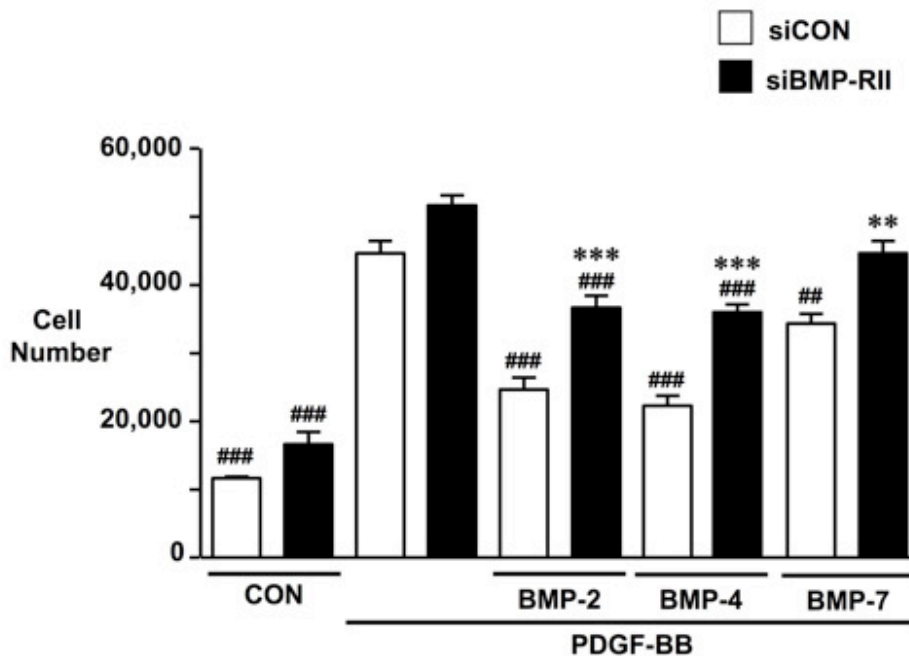
Hemodynamic Measurements in Mice. RV catheterisation: A 1.4 F catheter (Millar Instruments, Houston, Texas) was inserted into the right jugular vein and then placed into the RV free cavity, as previously described (11). Using the PowerLab/4SP recording unit (AD Instruments, Colorado Springs, CO), 3-5 tracings at different time points were averaged to determine the RVSP, maximal rate of pressure development (dp/dt max.; RV systolic function) and maximal rate of pressure decay (dp/dt min.; RV diastolic function). *Systemic blood pressure measurements (tail cuff method):* At least 5 recordings per mouse were averaged to determine systolic BP, MAP and diastolic BP. *Echocardiography:* Fractional shortening (FS) and heart rate (HR) were determined in M-mode. Ejection fraction (EF) and cardiac output (CO) were estimated using the Teichholz formula (12).

Lung tissue preparation. After abdominal aortic dissection, lungs were perfused in vivo by injecting 5ml normal saline into the beating RV. Lungs were tracheally injected with 10% formalin, fixed overnight, and then embedded either in paraffin for standard histology (Hematoxylin & Eosin, Elastic van Gieson, Movat pentachrome). Prior to fixation, a subset of left lungs were infused with barium-gelatin via the central PA (13) to label peripheral pulmonary arteries for morphometric analysis. The barium was infused by hand with similar endpoints of pre-capillary filling of all small vessels at alveolar duct and wall level. The total number of peripheral arteries was calculated as a ratio of number of arteries per surface area (5 random fields per slide) and per 100 alveoli in each field (200x magnification). Muscularized and non-muscularized peripheral (alveolar wall) pulmonary arteries were counted at 400x magnification in 5 random fields per lung. (200x magnification = 1 field)

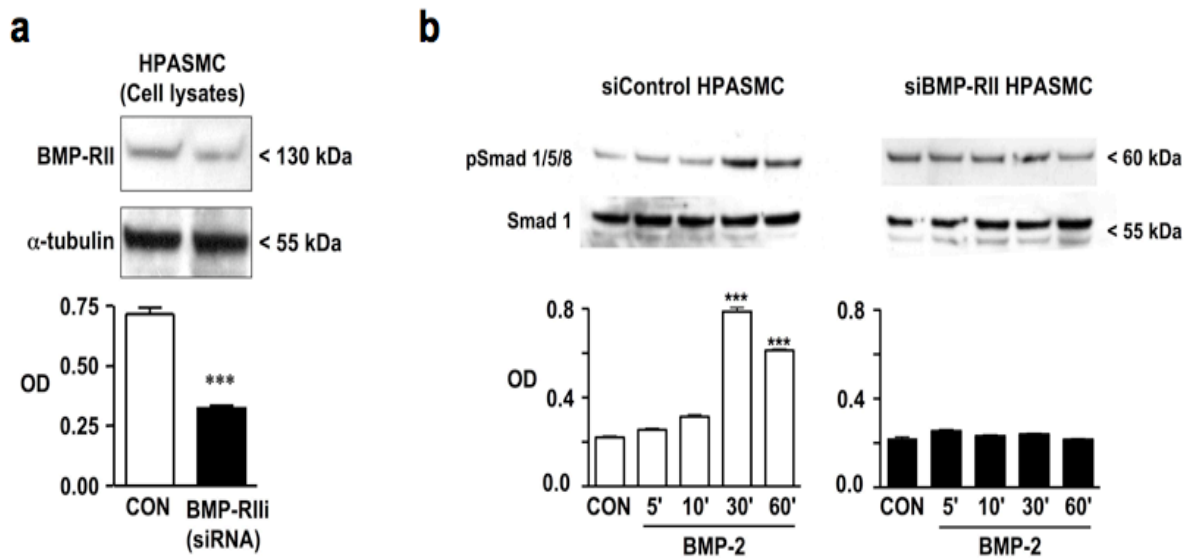
SUPPLEMENTARY DATA



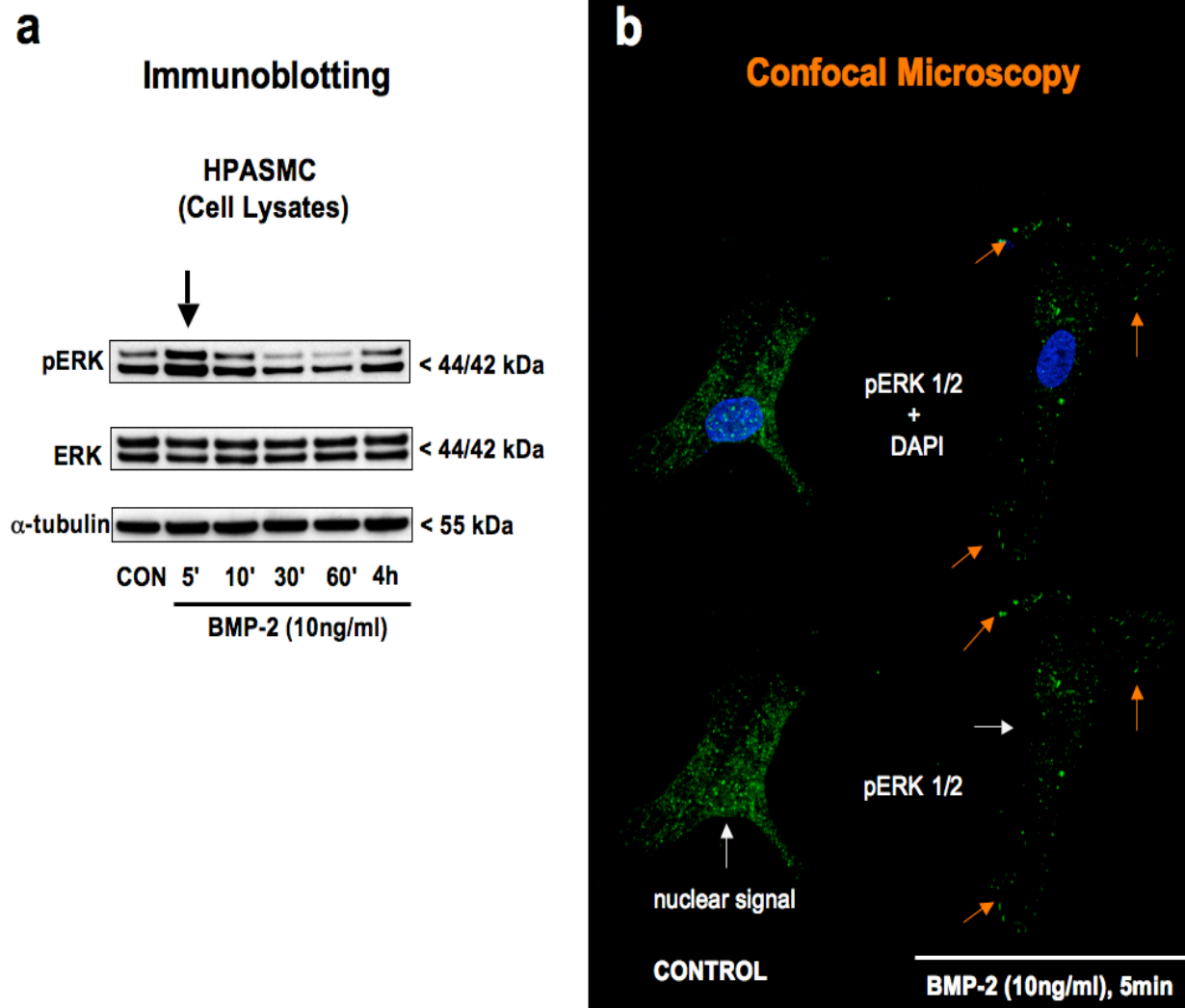
Supplementary Figure 2 BMP-2 (**a,c**), the PPAR γ agonist rosiglitazone (**b**), and apolipoprotein E (**d**) inhibit proliferation of human pulmonary artery smooth muscle cells (PASMC) induced by PDGF-BB (20ng/ml). **a**, Recombinant BMP-2 inhibits proliferation in LacZi control but not in shBMP2i PASMC in which BMP-receptor II expression is suppressed by shRNAi pLenti 6. **b**, Rosiglitazone (1 μ M) blocks human PASMC proliferation. The expansion of the y axis reflects higher baseline OD values. **c**, The inhibitory effect of BMP-2 on human PASMC proliferation is lost in the presence of the irreversible PPAR γ antagonist GW9662 (1 μ M). **d**, recombinant apolipoprotein E (apoE 10 μ M) inhibits human PASMC proliferation. Starvation, stimulation with PDGF-BB and MTT assay as described under methods. Bars represent mean \pm SEM (n = 4-8; n = 12-14 for PDGF-BB in Fig. 2b and 2d). * p < 0.05; *** p < 0.001.



Supplementary Figure 3 Antiproliferative effects of BMP-2, BMP-4, and BMP-7 in sicontrol and siBMP-RII (knock down) human PASCs. To achieve effective gene knockdown, siRNA duplexes specific for BMP-RII were transfected into human PASCs using Lipofectamine 2000 (Invitrogen). Knock-down efficiency was evaluated 48 hours later by measuring protein levels in cell lysates by western immunoblotting. Transfection of nontargeting siRNA duplexes (siCONTROL, Dharmacon, Inc) was performed simultaneously to serve as a control in all experiments. PASCs were seeded at 2.5×10^4 cells per well of a 24-well plate in 500 μ l of growth medium and allowed to adhere overnight. The cells were washed with PBS prior to the addition of starvation media (0.1% FBS) and incubated for 48h, and then stimulated with PDGF-BB (20ng/ml) for 72h. BMP-2, BMP-4 and BMP-7 (all 10ng/ml) were added to quiescent cells 30min. prior to PDGF-BB stimulation. Cell numbers in controls at time points 0h and 72h were not significantly different. Bars represent mean \pm SEM (n = 3). ANOVA with Bonferroni's multiple comparison test. ## p < 0.01; ### p < 0.001 denote comparisons with PDGF-BB stimulation of either siCON or siBMP-RII cells, in the absence of BMPs. * p < 0.05; ** p < 0.01; *** p < 0.001 denote comparisons between siCON and siBMP-RII for each ligand (BMP-2, BMP-4, BMP-7).



Supplementary Figure 4. Knock-down of human BMP-RII prevents BMP-2 mediated phosphoSmad 1/5/8 (pSmad 1/5/8) signalling in human PASC. **a**, Knock-down of human BMP-RII protein expression by small interfering RNA in human PASC. To achieve effective gene knockdown, siRNA duplexes specific for BMP-RII were transfected into human PASCs using Lipofectamine 2000. Nontargeting siRNA duplexes were used for control transfections (see Supplementary Methods). **b**, BMP-2 (10ng/ml) stimulation for 30min. induces Smad1/5/8 phosphorylation in siControl but not in siBMP-RII (knock-down) human PASC. Of note, Smad 1/5/8 phosphorylation occurs after BMP-2 mediated activation of PPAR γ (see Figure 2d, main manuscript). Cell culture, total cell lysate preparation and Western immunoblotting are described in the (Supplementary) Methods section. Arbitrary OD values (densitometry): Bars represent mean \pm SEM (n = 3). Unpaired two-tailed t-test (**a**) and ANOVA with Bonferroni's multiple comparison test (**b**). *** p < 0.001 versus control.



Supplementary Figure 5. BMP-2 induces rapid extra-nuclear ERK1/2 phosphorylation that is accompanied by a strong signal at the cytoplasmic membrane. **a**, Western immunoblotting of total cell lysates: pERK1/2, total ERK1/2, and α -tubulin (2nd loading control). Human PASMC were stimulated with BMP-2 (10ng/ml) for 5-60min., and 4h (n=2). Cell culture and preparation of total cell lysates (which include the cytoplasmic membrane fraction) as described in the Methods section. **b**, Immunohistochemistry/Confocal microscopy. DAPI = nuclear DNA stain, bright green = pERK1/2 stain (see Supplementary Methods section). BMP-2 stimulation (5min.) impairs the nuclear signal of pERK (white arrows). This is accompanied by strong pERK 1/2 staining at the cytoplasmic membrane (orange arrows; see also Figure 2b, main manuscript).

References (Supplement)

1. Hevener, A.L., He, W., Barak, Y., Le, J., Bandyopadhyay, G., Olson, P., Wilkes, J., Evans, R.M., and Olefsky, J. 2003. Muscle-specific Pparg deletion causes insulin resistance. *Nat Med* 9:1491-1497.
2. Fouty, B.W., Grimison, B., Fagan, K.A., Le Cras, T.D., Harral, J.W., Hoedt-Miller, M., Sclafani, R.A., and Rodman, D.M. 2001. p27(Kip1) is important in modulating pulmonary artery smooth muscle cell proliferation. *Am J Respir Cell Mol Biol* 25:652-658.
3. Yang, X., Long, L., Southwood, M., Rudarakanchana, N., Upton, P.D., Jeffery, T.K., Atkinson, C., Chen, H., Trembath, R.C., and Morrell, N.W. 2005. Dysfunctional Smad signaling contributes to abnormal smooth muscle cell proliferation in familial pulmonary arterial hypertension. *Circ Res* 96:1053-1063.
4. Wharton, J., Davie, N., Upton, P.D., Yacoub, M.H., Polak, J.M., and Morrell, N.W. 2000. Prostacyclin analogues differentially inhibit growth of distal and proximal human pulmonary artery smooth muscle cells. *Circulation* 102:3130-3136.
5. Morrell, N.W., Yang, X., Upton, P.D., Jourdan, K.B., Morgan, N., Sheares, K.K., and Trembath, R.C. 2001. Altered growth responses of pulmonary artery smooth muscle cells from patients with primary pulmonary hypertension to transforming growth factor-beta(1) and bone morphogenetic proteins. *Circulation* 104:790-795.
6. Morrell, N.W., Upton, P.D., Kotecha, S., Huntley, A., Yacoub, M.H., Polak, J.M., and Wharton, J. 1999. Angiotensin II activates MAPK and stimulates growth of human pulmonary artery smooth muscle via AT1 receptors. *Am J Physiol* 277:L440-448.
7. Dignam, J.D., Lebovitz, R.M., and Roeder, R.G. 1983. Accurate transcription initiation by RNA polymerase II in a soluble extract from isolated mammalian nuclei. *Nucleic Acids Res* 11:1475-1489.
8. Mitani, Y., Zaidi, S.H., Dufourcq, P., Thompson, K., and Rabinovitch, M. 2000. Nitric oxide reduces vascular smooth muscle cell elastase activity through cGMP-mediated suppression of ERK phosphorylation and AML1B nuclear partitioning. *Faseb J* 14:805-814.
9. Hodge, D.R., Peng, B., Pompeia, C., Thomas, S., Cho, E., Clausen, P.A., Marquez, V.E., and Farrar, W.L. 2005. Epigenetic silencing of manganese superoxide dismutase (SOD-2) in KAS 6/1 human multiple myeloma cells increases cell proliferation. *Cancer Biol Ther* 4:585-592.
10. Shurin, G.V., Ferris, R.L., Tourkova, I.L., Perez, L., Lokshin, A., Balkir, L., Collins, B., Chatta, G.S., and Shurin, M.R. 2005. Loss of new chemokine CXCL14 in tumor tissue is associated with low infiltration by dendritic cells (DC), while restoration of human CXCL14 expression in tumor cells causes attraction of DC both in vitro and in vivo. *J Immunol* 174:5490-5498.
11. Hansmann, G., Wagner, R.A., Schellong, S., Perez, V.A., Urashima, T., Wang, L., Sheikh, A.Y., Suen, R.S., Stewart, D.J., and Rabinovitch, M. 2007. Pulmonary arterial hypertension is linked to insulin resistance and reversed by peroxisome proliferator-activated receptor-gamma activation. *Circulation* 115:1275-1284.
12. Teichholz, L.E., Kreulen, T., Herman, M.V., and Gorlin, R. 1976. Problems in echocardiographic volume determinations: echocardiographic-angiographic correlations in the presence of absence of asynergy. *Am J Cardiol* 37:7-11.
13. Ye, C.L., and Rabinovitch, M. 1991. Inhibition of elastolysis by SC-37698 reduces development and progression of monocrotaline pulmonary hypertension. *Am J Physiol* 261:H1255-1267.